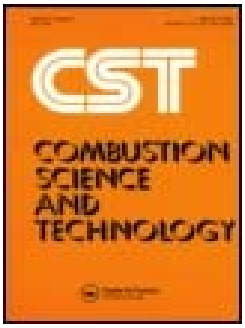

Combustion Science and Technology

ISSN: 0010-2202 (Print) 1563-521X (Online) Journal homepage: https://www.tandfonline.com/loi/gcst20

Combustion with Multiple Flames under High Strain Rates

William A. Sirignano

To cite this article: William A. Sirignano (2019): Combustion with Multiple Flames under High Strain Rates, Combustion Science and Technology, DOI: 10.1080/00102202.2019.1685507

To link to this article: https://doi.org/10.1080/00102202.2019.1685507

COMBUSTION SCIENCE AND TECHNOLOGY
https://doi.org/10.1080/00102202.2019.1685507

Combustion with Multiple Flames under High Strain Rates

William A. Sirignano

Department of Mechanical and Aerospace Engineering, University of California, Irvine, CA, USA

ABSTRACT

Structures with multiple flames, nonpremixed and premixed, in strained flow representative of turbulent combustion are analyzed with reacting, viscous, three-dimensional counterflows. There can be differing normal strain rates in each of the three directions. Special attention is given to configurations with a diffusion flame plus one or two partially premixed flames. Reduction of the equations to a similar form is obtained allowing for variations in density due to temperature, heat conduction, and mass diffusion. Solutions to the Navier-Stokes equations are obtained without the boundary-layer approximation. In steady, variable-density configurations, a set of ODEs governs the two transverse velocity components and the axial velocity component, as well as the scalar-field variables. Results for the velocity and scalar fields are found for a full range of the distribution of normal strain rates between the two transverse directions, a very wide range of Damköhler number *Da* based on strain rate, and various Prandtl number values. As strain rate is increased and/or pressure decreases, the multiple flames will merge into a single diffusion flame. With further changes in that direction, extinction will occur. In the three-flame case, the fuel-rich premixed flame merges first with the diffusion flame as *Da* decreases; then with further decrease, the fuel-lean premixed flame merges with the diffusion flame, leaving just a diffusion flame that will extinguish with further decrease. Velocity overshoots are seen in the viscous layer, yielding an important correction of theories based on a constant-density assumption. Advection and convection are important in the neighborhood of the flames.

ARTICLE HISTORY
Received 5 July 2019
Revised 23 October 2019
Accepted 23 October 2019

KEYWORDS
flamelet theory; three-dimensional counterflow combustion; multi-branched flames

Introduction

There is a growing interest in understanding the laminar mixing and combustion that commonly occurs within turbulent eddies. These laminar flamelet sub-domains experience significant strain. Some important work has been done here but typically in two-dimensions or axisymmetry and often with a constant-density approximation. See Linan (1974), Marble (1985), Karagozian and Marble (1986), Cetegen and Sirignano (1988, 1990)), Peters (2000), and Pierce and Moin (2004). Linan and Peters focused on the counterflow configuration. Karagozian and Marble did examine a three-dimensional strained-flow configuration where flow moved radially inward and jetted axially outward; in addition, a vortex had the same axis as the flow. The vortex caused the diffusion flame sheet to wrap around the axis. Pierce and Moin modified the counterflow configuration by fixing domain size and forcing flux to zero at the boundaries. They are all built around the postulate that the flamelets are always nonpremixed (i.e., diffusion) flames and subject to

CONTACT William A. Sirignano sirignan@uci.edu Department of Mechanical and Aerospace Engineering, University of California, Irvine, CA, USA

flow strain. Nguyen, Popov, and Sirignano (2018) and Nguyen and Sirignano (2018) employed the Pierce-Moin flamelet approach in the simulation of a single-injector rocket engine. They showed the importance of flamelets subject to high strain rates. However, contradictions appeared in that both premixed flames and nonpremixed flames appeared in the predictions. In fact, they report multi-branched flames; in particular, the combination is often seen of a fuel-lean premixed-flame branch with a branch consisting of a merged diffusion flame and fuel-rich premixed flame.

Hamins, Thridandam, and Seshadri (1985) showed through experiment and asymptotic analysis that a partially premixed fuel-lean flame and a diffusion flame can co-exist in a counterflow where a stream of heptane vapor opposed a stream of a methane-oxygen-nitrogen mixture. Flame merging and extinction occurred as the fraction of nitrogen in the stream was increased. Clearly, a need exists to expand the flamelet theory to address both premixed and non-premixed flames. Recently, Rajamanickam et al. (2019) have provided an interesting three-dimensional triple-flame analysis; the imposed strain however is limited to two dimensions.

There is a strong need to study mixing and combustion in counterflows where the imposed strain is three-dimensional. In this work, we extend flamelet theory in two significant aspects: the inclusion of both premixed and non-premixed flame structures and the extension to three-dimensional strained flow fields. No claim is made about the completeness and finality of our work here toward that goal. Still, some important issues are clarified.

Here, we address a set of steady three-dimensional counterflows under certain constraints, with combustion and variable density and properties. A three-dimensional, non-axisymmetric counterflow is treated with differing strain rates in each direction whereby the flow can have greater acceleration in one transverse direction than in the other. The classical treatment by Peters (2000) has two opposing streams, one of fuel or fuel plus a chemically inert gas and the other of oxidizer or oxidizer plus an inert gas. We focus on situations where one or both of inflowing streams consists of a combustible mixture of fuel and oxidizer. Specifically, we treat three cases: a fuel-lean mixture flowing against pure fuel, a fuel-rich mixture flowing against pure oxygen, and a fuel-rich mixture flowing against a fuel-lean mixture. These various configurations have interesting differences as well as similarities. For comparisons, a singe-premixed-flame case and a single-diffusion-flame case are also presented. Propane and oxygen are considered with one-step, Westbrook and Dryer (1984) kinetics; however, the conclusions are expected to be more general. Consideration of detailed kinetics and evaluation of related subtleties that are likely to appear can occur in the following works once the potential for existence of multiple flames in the counterflow configuration is demonstrated here. Those one-step kinetic relations were obtained by fitting to experiments for premixed flames and are expected to be less accurate for diffusion flames. However, we can tolerate some error here because kinetics are not rate controlling for diffusion flames. The approach here expands on recent work by Sirignano (2019) which used infinite kinetics for three-dimensional counterflow diffusion flames.

In the next section, the analysis is presented with results following in several sections. In order, the results for five types of reacting counterflows are presented in Sections 3 through 7: the simple diffusion flame as a reference case, the simple premixed flame as a second reference case, a configuration with a premixed fuel-lean flame and diffusion

flame, another configuration with a premixed fuel-rich flame and diffusion flame, and a three-flame configuration. In Section 8, the relevance of these new findings for flamelet theory is discussed.

Analysis

The counterflow configuration has been widely used in combustion studies. It represents the correct asymptotic behavior near a stagnation point for a flame under normal strain. It offers the convenience of yielding a system of ordinary differential equations to describe a multi-dimensional configuration. Consider, for example, a counterflow from both the negative y-direction and positive y-direction with outflow in the x- and z-directions, the interface along $y = 0$, and a stagnation point at $x = y = z = 0$. The velocity $\vec{u}$ has the components $u, \mathrm{v},$ and w in the $x, y,$ and z directions, respectively. The y-direction has arbitrarily been chosen here to be the only direction with the negative strain rate. The z-direction arbitrarily has the larger (or equal) positive strain rate while the x-direction has a smaller, equal, or zero normal strain rate. If the approaching streams have the same pressure at a distance from the interface and its viscous layer, we expect that, in a frame of reference attached to the interface, momentum balance for steady flow yields $\rho_{-\infty}\mathrm{v}_{-\infty}^2 = \rho_{\infty}\mathrm{v}_{\infty}^2$. The incoming flow is in the direction of decreasing y-magnitude. The normal strain rates in the x- and z-directions are $S_1 = \partial u/\partial x|_{x=\infty}$ and $S_2 = \partial w/\partial z|_{z=\infty}$, respectively. Here, for the nondimensional variables to be defined below and given by Sirignano (2019), $S_1 + S_2 = 1$, $0.5 \geq S_1 \geq 0$, and $1 \geq S_2 \geq 0.5$. These normal strain rates for these two opposing streams will match at the interface $y = 0$ since the velocity components are continuous there. The y-directed inflowing streams in all cases bring together fluids of differing temperature and/or composition; so, heat diffusion and mass diffusion are in the y-direction.

The two streams need not have the same upstream values for velocity v, temperature T, enthalpy h, density ρ, or composition reflected through mass fraction Y_m for chemical species m. Pressure p will be given the same upstream values for the two streams. Fickian mass diffusion and Fourier heat conduction are considered so that all fluid properties are continuous across the interface. Radiation and gravity are neglected.

The governing equations for unsteady 3D flow are given as

$$\frac{\partial \rho}{\partial t} + \frac{\partial (\rho u_j)}{\partial x_j} = 0 \tag{1}$$

$$\rho \frac{\partial u_i}{\partial t} + \rho u_j \frac{\partial u_i}{\partial x_j} + \frac{\partial p}{\partial x_i} = \frac{\partial \tau_{ij}}{\partial x_j} \tag{2}$$

where, following the Stokes hypothesis for a Newtonian fluid,

$$\tau_{ij} = \mu \left[\frac{\partial u_i}{\partial x_j} + \frac{\partial u_j}{\partial x_i} - \frac{2}{3}\delta_{ij} \frac{\partial u_k}{\partial x_k} \right] \tag{3}$$

$$\rho\frac{\partial h}{\partial t}+\rho u_j\frac{\partial h}{\partial x_j}-\frac{\partial p}{\partial t}-u_j\frac{\partial p}{\partial x_j}=\frac{\partial}{\partial x_j}\left(\frac{\lambda}{c_p}\frac{\partial h}{\partial x_j}\right)+\frac{\partial}{\partial x_j}\left(\rho D(1-Le)\Sigma_{m=1}^{N}h_m\frac{\partial Y_m}{\partial x_j}\right)$$
$$-\rho\Sigma_{m=1}^{N}h_{f,m}\omega_m+\tau_{ij}\frac{\partial u_i}{\partial x_j} \tag{4}$$

$$\rho\frac{\partial Y_m}{\partial t}+\rho u_j\frac{\partial Y_m}{\partial x_j}=\frac{\partial}{\partial x_j}\left(\rho D\frac{\partial Y_m}{\partial x_j}\right)+\rho\omega_m;\quad m=1,2,....,N \tag{5}$$

The Lewis number $Le=1$ is considered. With neglect of terms of the order of the Mach number squared, the energy equation (4) is simplified as follows:

$$\rho\frac{\partial h}{\partial t}+\rho u_j\frac{\partial h}{\partial x_j}-\frac{\partial p}{\partial t}=\frac{\partial}{\partial x_j}\left(\rho D\frac{\partial h}{\partial x_j}\right)-\rho\Sigma_{m=1}^{N}h_{f,m}\omega_m \tag{6}$$

Here, the sensible enthalpy $h=c_pT$ based on the assumption of a calorically perfect gas. When normalized by ambient conditions, the nondimensional values of enthalpy and temperature are identical. For simplification, we neglect the effect of species composition on specific heats and the specific gas constant. For the one-step kinetics considered here, the last term in Equation (6) may be replaced by $\rho Q\omega_F$ where Q is the heating value (energy/mass) of the fuel and ω_F is the chemical oxidation rate of the fuel.

The nondimensional forms of the above equations remain identical to the above forms if we choose certain reference values for normalization. In the remainder of this article, the nondimensional forms of the above equations will be considered. The superscript * will be used to designate a dimensional property. The variables $u_i^*, t^*, x_i^*, \rho^*, h^*, p^*,$ and $\omega_m^*,$ and properties $\mu^*, \lambda^*/c_p^*,$ and D^* are normalized respectively by $[(S_1^*+S_2^*)\mu_\infty^*/\rho_\infty^*]^{1/2}, (S_1^*+S_2^*)^{-1}, [\mu_\infty^*/(\rho_\infty^*(S_1^*+S_2^*))]^{1/2}, \rho_\infty^*, (S_1^*+S_2^*)\mu_\infty^*/\rho_\infty^*, (S_1^*+S_2^*)\mu_\infty^*, (S_1^*+S_2^*), \mu_\infty^*,\ \mu_\infty^*,$ and $\mu_\infty^*/\rho_\infty^*$. It is understood that, for unsteady flow, the reference values for strain rates and far-stream variables and properties used for normalization will be constants. Note that the reference length $[\mu_\infty^*/(\rho_\infty^*(S_1^*+S_2^*))]^{1/2}$ is the estimate for the magnitude of the viscous-layer thickness.

The stagnation point in the steady counterflow will be taken as the origin $x=y=z=0$. Along the line $x=z=0$ normal to the interface, we can expect the first derivatives of $\mathrm{v}, \rho, \mathrm{h}, \mathrm{T},$ and Y_m with respect to either x or z to be zero-valued. The velocity components u and w there will be odd functions of x and z, respectively, going through zero and changing sign at that line. Consequently, upon neglect of terms of $O(x^2)$ and $O(z^2)$, the variables $\mathrm{v}, \rho, \mathrm{h}, \mathrm{T},$ and Y_m can be considered to be functions only of y. The density-weighted Illingworth transformation of y can be used to replace y with $\eta\equiv\int_0^y\rho(y')dy'$. Neglect of the same order of terms implies that $u=S_1x(df_1/d\eta)$ and $w=S_2z(df_2/d\eta)$. Note u is independent of z and w is independent of x in this case where no shear strain is imposed on the incoming stream(s). At the edge of the viscous layer at large positive η, $df_1/d\eta\to1, df_2/d\eta\to1, f_1\to\eta,$ and $f_2\to\eta$.

We define $()'\equiv d()/d\eta$. In the nondimensional form given by Equations (1) through (6), the dimensional strain rates S_1^* and S_2^* are each normalized by the dimensional sum

$S_1^* + S_2^*$. Thus, the nondimensional relation is $S_2 = 1 - S_1$ and only one independent nondimensional strain-rate parameter is needed. Nevertheless, two strain rates are presented above and in the following analysis with the understanding that one depends on the other such that $S_1 + S_2 = 1$. $S_1 + S_2$ will be explicitly stated in our analysis without substitution of the unity value. This choice clarifies whether a particular term when converted to a dimensional form depends on S_1^*, S_2^*, or the sum of the two strain rates. The quantity $S_1^* + S_2^*$ will be embedded in a Damköhler number *Da*.

In the physical counterflow description, there are four characteristic times: chemical time, flow residence time within the viscous layer (i.e., reciprocal of strain rate), heat diffusion time, and mass diffusion time. With our assumption that $Le = 1$, the last two times are identical. Then, for the special case where $Pr = 1$, the last three times become identical. For the range of *Pr* values considered here, the magnitude order of these three times remain the same. The two independent nondimensional ratios given by the chemical, residence, and diffusion times are *Da* and *Pr*.

For steady state, the continuity equation (1) is readily integrated to give

$$\rho \mathrm{v} = -\mathrm{S}_1 \mathrm{f}_1(\eta) - \mathrm{S}_2 \mathrm{f}_2(\eta) \tag{7}$$

and then

$$\frac{d\mathrm{v}}{d\eta} = \frac{S_1 f_1(\eta) + S_2 f_2(\eta)}{\rho^2} \frac{d\rho}{d\eta} - \frac{S_1 f_{1'}(\eta) + S_2 f_{2'}(\eta)}{\rho} \tag{8}$$

Thus, the incoming inviscid flow outside the boundary layer is described by $\mathrm{v} = -(\mathrm{S}_1 + \mathrm{S}_2)\eta$ for positive η and $\mathrm{v} = -(\mathrm{S}_1 + \mathrm{S}_2)\eta/\rho_{-\infty}$ for negative η. Then, $\mathrm{v} = -(\mathrm{S}_1 + \mathrm{S}_2)\mathrm{y}$ for the external incoming flow.

As shown by Sirignano (2019), we obtain in the steady state, with the assumptions that $\rho\mu = 1$, $\tilde{h} \equiv h/h_\infty$, and a perfect-gas law that relates enthalpy with density

$$\begin{gathered} f'''_1 + (S_1 f_1 + S_2 f_2) f''_1 + S_1(\tilde{h} - (f'_1)^2) = 0 \\ f'''_2 + (S_1 f_1 + S_2 f_2) f''_2 + S_2(\tilde{h} - (f'_2)^2) = 0 \\ f'_1(\infty) = \sqrt{\rho_{-\infty}} f'_1(-\infty) = f'_2(\infty) = \sqrt{\rho_{-\infty}} f'_2(-\infty) = 1\ ; \\ f_1(0) = f_2(0) = 0 \end{gathered} \tag{9}$$

where

$$\begin{aligned} \mathrm{v}(\infty) &= -(\mathrm{S}_1 + \mathrm{S}_2)\eta = -(\mathrm{S}_1 + \mathrm{S}_2)\mathrm{y}\ ; \\ \mathrm{v}(-\infty) &= -(\mathrm{S}_1 + \mathrm{S}_2)\frac{\eta}{\rho_{-\infty}^{3/2}} = -(\mathrm{S}_1 + \mathrm{S}_2)\frac{\mathrm{y}}{\sqrt{\rho_{-\infty}}} \end{aligned} \tag{10}$$

Here, the ambient temperature of both incoming streams has been assumed to be identical; thus, $\rho_{-\infty} = 1$. Note that the variation of pressure through the counterflow has been taken to have no consequence for the energy equation, transport properties, and equations of state. $S_1 + S_2 = 1$ in the steady, nondimensional representation. It is left without simplification to emphasize that the particular distribution of strain between the *x* and *z* directions does not matter.

In general, each of the species equations must be solved. However, for the special case assumed here of a one-step chemical reaction, each species is consumed or produced at a rate in direct proportion to the rate of some other species that is produced or consumed. Therefore, the steady-state version of Equation (5) with $Le = 1$ for fuel mass fraction Y_F and oxygen mass fraction Y_O can be written as

$$\begin{aligned} Y''_F + Pr(S_1 f_1 + S_2 f_2) Y'_F &= Pr\omega_F \\ Y''_O + Pr(S_1 f_1 + S_2 f_2) Y'_O &= Pr\omega_F / \nu \\ Y_F(\infty) = Y_{F,\infty};\quad Y_F(-\infty) &= Y_{F,-\infty} \\ Y_O(\infty) = Y_{O,\infty};\quad Y_O(-\infty) &= Y_{O,-\infty} \end{aligned} \tag{11}$$

where ν is a mass stoichiometric constant. For the steady-state energy equation, we have from Equation (6)

$$\begin{aligned} \tilde{h}'' + Pr(S_1 f_1 + S_2 f_2)\tilde{h}' &= Pr\tilde{Q}\omega_F \\ \tilde{h}(\infty) = 1;\quad \tilde{h}(-\infty) &= \frac{1}{\rho_{-\infty}} \end{aligned} \tag{12}$$

where $\tilde{Q}$ is the fuel heating value normalized by the enthalpy at plus infinity. For a perfect gas with constant specific heat, the nondimensional enthalpy $\tilde{h}$ also equals the temperature normalized by the temperature at plus infinity.

Equations (9) indicates a dependence of the heat and mass transport on $f \equiv S_1 f_1 + S_2 f_2$. Thus, the behavior for the counterflow can vary from the planar values of $S_1 = 1$ and $S_2 = 0$ (or vice versa) or from the axisymmetric case $S_1 = S_2 = 1/2$.

The dependence of v on $f \equiv S_1 f_1 + S_2 f_2$ is shown by Equation (7). Thus, the function f will be important in determining both the field for v and the scalar fields and will generally depend on both S_1 and S_2, not merely on $S_1 + S_2$. The particular distribution of the normal strain rate between the two transverse directions matters. In our calculations, attention is placed on the planar case ($S_1 = 0, S_2 = 1.0$) where the product $S_1 S_2$ is minimized, a fully three-dimensional case ($S_1 = 0.25, S_2 = 0.75$), and the axisymmetric case ($S_1 = S_2 = 0.5$) where the product $S_1 S_2$ is maximized. The reasons for bounding the parameter ($0 \le S_1 \le 0.5$) is that S_1 and S_2 together with x and z can be interchanged to get results for the range $0 \le S_1 \le 1.0$.

The values of v do not asymptote to a constant at $+\infty$ or $-\infty$ but rather relax to an inviscid potential flow; we therefore will take the boundary values for ν at y^* positions whose magnitudes are severalfold the expected viscous-layer thickness, $[\mu^*_\infty/(\rho^*_\infty(S_1^* + S_2^*))]^{1/2}$. So, $+\infty$ is approximated by a value of $y >> 1$ or $\eta >> 1$ while $-\infty$ is approximated by a value of $|y| >> 1$ or $|\eta| >> \rho_{-\infty}$. Compressibility effects within the viscous layer will be assumed to be negligible but density change due to temperature will be considered. The magnitude of the dimensional velocity at the layer edge is $[(S_1^* + S_2^*)\mu^*_\infty/\rho^*_\infty]^{1/2}$; thus, the kinetic energy per mass based will be assumed to be small compared to the ambient enthalpy values, simplifying the energy equation.

We define the Shvab-Zel'dovich variables $\alpha \equiv Y_F - \nu Y_O$ and $\beta \equiv \tilde{h} + \nu Y_O \tilde{Q}$ where $\tilde{Q}$ is the fuel heating value normalized by $h^*(\infty)$. Then, we have

$$\begin{gathered}\alpha'' + Pr(S_1 f_1 + S_2 f_2)\alpha' = 0 \\ \beta'' + Pr(S_1 f_1 + S_2 f_2)\beta' = 0 \\ \alpha(\infty) = 1\ ;\ \ \alpha(-\infty) = -\nu \\ \beta(\infty) = 1\ ;\ \ \beta(-\infty) = \frac{1}{\rho_{-\infty}} + \nu\tilde{Q} = \frac{h_{-\infty}}{h_\infty} + \nu\tilde{Q}\end{gathered} \tag{13}$$

The above equations can be readily applied for diffusion-flame counterflows and partially-premixed-flame counterflows as will be explained in the following sections. We will focus on propane-oxygen flows with one-step kinetics. However, results are expected to be qualitatively more general, applying to situations with more detailed kinetics and to other hydrocarbon/oxygen-or-air combination. Westbrook and Dryer (1984) kinetics are used; they were developed for premixed flames but any error for nonpremixed flames is viewed as tolerable here because diffusion would be rate-controlling. One may deduce that

$$\omega_F^* = -A^* {\rho^*}^{0.75} Y_F^{0.1} Y_O^{1.65} e^{-50.237/\tilde{h}} \tag{14}$$

where the ambient temperature is set at 300 K and density ρ^* is to be given in units of kilograms per cubic meter. Here, $A^* = 4.79\text{x}10^8 (kg/m^3)^{-0.75}/s$. The dimensional strain rate $S_1^* + S_2^*$ is used to normalize time and reaction rate. In nondimensional terms,

$$\begin{aligned}\omega_F &= -\frac{A^* {\rho_\infty^*}^{0.75}}{S_1^* + S_2^*} \tilde{h}^{-0.75} Y_F^{0.1} Y_O^{1.65} e^{-50.237/\tilde{h}} \\ \omega_F &= -\frac{Da}{\tilde{h}^{0.75}} Y_F^{0.1} Y_O^{1.65} e^{-50.237/\tilde{h}}\end{aligned} \tag{15}$$

The above equation defines the Damköhler number Da. Furthermore, we set $Da \equiv K Da_{ref}$ where

$$Da_{ref} \equiv \frac{\tilde{A}(10 kg/m^3)^{0.75}}{(100/s)} = 2.693\ x\ 10^7;\ \ K \equiv \left[\frac{\rho_\infty^*}{10 kg/m^3}\right]^{0.75} \frac{100/s}{S_1^* + S_2^*} \tag{16}$$

$10\ kg/m^3$ and $100/s$ are arbitrarily chosen as reference values for density and strain rate, respectively. The reference value for density implies an elevated pressure. The strain-rate reference value is in the middle of an interesting range for this chemical reaction. Clearly, there is no need to set pressure (or its proxy, density) and the strain rate separately for a one-step reaction. For propane and oxygen, the mass stoichiometric ratio $\nu = 0.275$.

The nondimensional parameter K will increase (decrease) as the strain rate decreases (increases) and/or the pressure increases (decreases). $K = 1$ is our base case and the range covered will include $10^{-3} \leq K \leq 10$.

The system of ordinary differential equations is solved numerically using a relaxation method and central differences. Solution over the range $-4 \leq \eta \leq 4$ provides adequate fittings to the asymptotic behaviors. The parameters that are varied are $K, Pr,$ and S_1 (and thereby $S_2 = 1 - S_1$). Most calculations have $Pr = 1$ and $S_1 = 0.25$ with emphasis on the effect of variation in K, i.e., pressure and strain rate. However, the effects of Pr and S_1 variations are shown as well. The ambient temperatures in the two incoming streams are

taken to be identical here. Sirignano (2019) has shown that the difference can have some importance on the flow. Five qualitatively different cases are examined in the following five sections. In all cases, the temperatures, densities, and enthalpies of the two ambient incoming flows are identical to each other.

Single diffusion flame

The well-known diffusion-flame case is discussed first to provide a reference case. For the case of a simple diffusion flame with Y_F and Y_O representing the mass fractions of fuel and oxidizer, the conserved scalar is $\alpha = Y_F - \nu Y_O$. The far incoming stream on one side (positive y and η) has $Y_F = 1$ while the other far incoming stream (negative y and η) has $Y_O = 1$. Scalar properties are shown in Figure 1 for K (and therefore Da) varying over four orders of magnitude. The three-dimensional case with $S_1 = 0.25$ and $S_2 = 0.75$ is examined. The behavior is that of a classical example of a nonpremixed (i.e., diffusion) flame with fuel approaching the flame from one side and oxygen from the other side through the algebraic sum of advective and diffusive fluxes.

The reaction zone and therefore the peak values of temperature and enthalpy occur on the negative (oxygen) side of the flow interface. For $K \geq 10^{-1}$, thin-diffusion-flame character is seen. Below that value (higher strain rate and/or lower pressure), extinction is seen to be underway. The effect on the conserved scalars α and β is modest and appears only indirectly through the velocity field. In Figure 2, it is seen that velocity overshoots occur in all three components as previously noted by Sirignano (2019). The peak of the v component of velocity occurs at the reaction zone while u and w peak closer to the stagnation plane. The strain rate in the y-direction is not everywhere negative; positive portions result with overshoot and greater-than-ambient values. In fact, the overshoot causes substantial increase for local strain rates near the flame. At the flame itself, the velocity derivative changes sign implying a local minimum value for the magnitude of the strain rate. At the reaction zone, the heat and mass diffusion (represented through second-derivative terms) dominate the convection and advection terms (represented through first derivative terms). However, advection as well as diffusion is significant in the near neighborhood of the flame. Models that would eliminate advection and convection have to be questioned. Furthermore, the constant-density assumption would miss several of these interesting effects.

Single premixed flame

Now, the premixed-flame case is analyzed to provide a second reference case. The far incoming stream on one side (positive y and η) has a stoichiometric mixture of propane and oxygen mixed with an inert gas ($Y_{F,\infty} = \nu Y_{O,\infty} = 0.1$) while the other far incoming stream (negative y and η) has a hot inert gas. Scalar properties are shown in Figure 3 while the velocity components are shown in Figure 4 for K (and therefore Da) varying over four orders of magnitude. The three-dimensional case with $S_1 = 0.25$ and $S_2 = 0.75$ is again examined.

Some of the general behaviors shown in Figures 3 and 4 are those expected for a classical premixed flame. As K (and therefore Da) decreases, the flame moves to a lower velocity region of the counterflow, the thicknesses of both the diffusive-

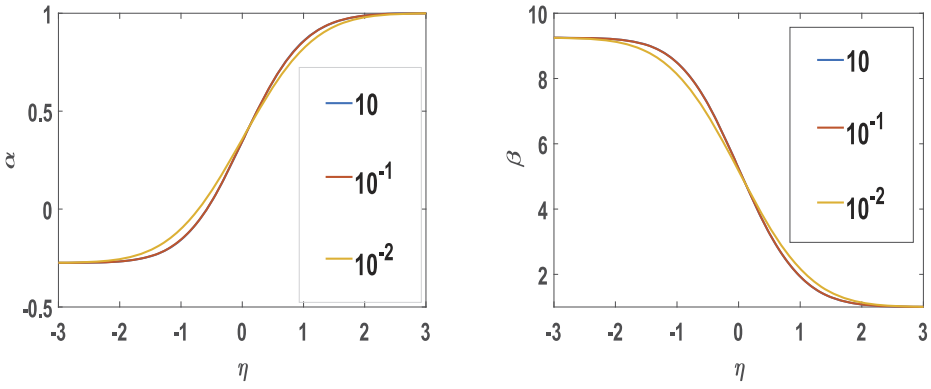

(a) α

(b) β

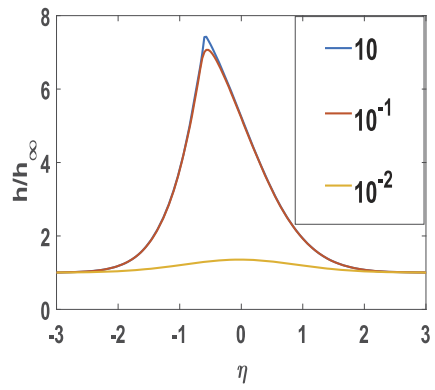

(c) $\tilde{h} = h/h_\infty$

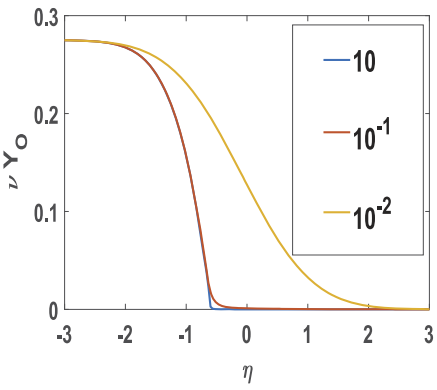

(d) νY_O

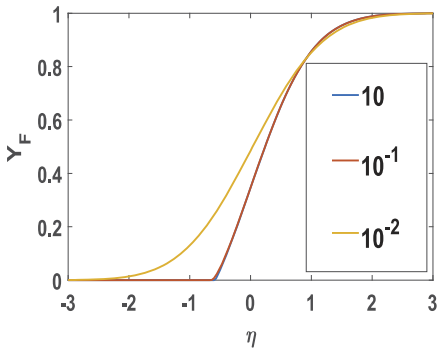

(e) Y_F

Figure 1. Single diffusion flame solutions with several strain-pressure parameter K values for nondimensional conserved scalars α, β; enthalpy h; and mass fractions $\nu Y_O, Y_F$. $Pr = 1.0; S_1 = 0.25, S_2 = 0.75$.

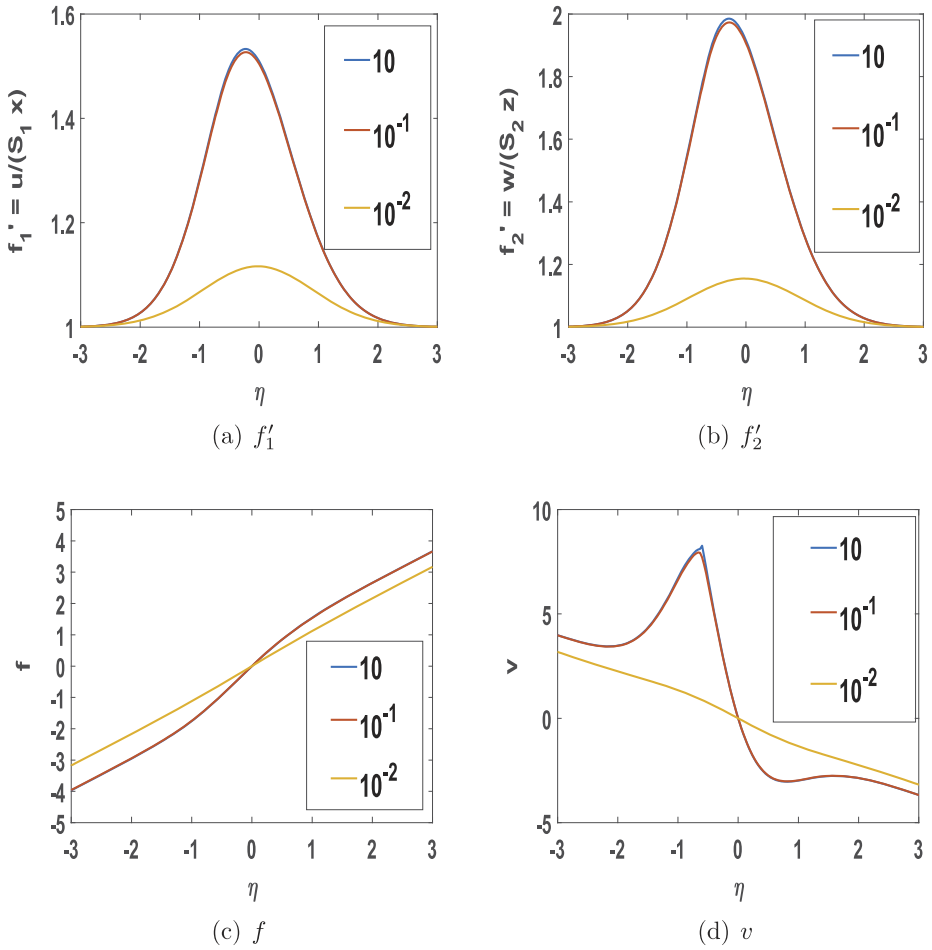

Figure 2. Single diffusion flame solutions with several strain-pressure parameter K values for non-dimensional variables f_1', f_2', f, v. $Pr = 1.0; S_1 = 0.25, S_2 = 0.75$.

advective region and the reaction zone increase, and the peak ω_F decreases. With continued decrease of K, i.e., increase of strain rate or decrease of pressure, extinction occurs. The reaction rate has essentially become negligible below some value in the range $0.01 < K < 0.1$. It must be understood that this counterflow situation differs from the one-dimensional premixed flame; the combustible species can only diffuse but not advect into the negative-η range because of the flow reversal. An interesting observation is that, with decreasing K, the reaction zone moves into the negative-y region while the diffusive-advective remains in the positive-y domain. This is possible because advection is not major in the reaction zone where a diffusive-reactive balance exists. Overshoot of each of the three velocity components is seen in the region where temperature rises and density decreases.

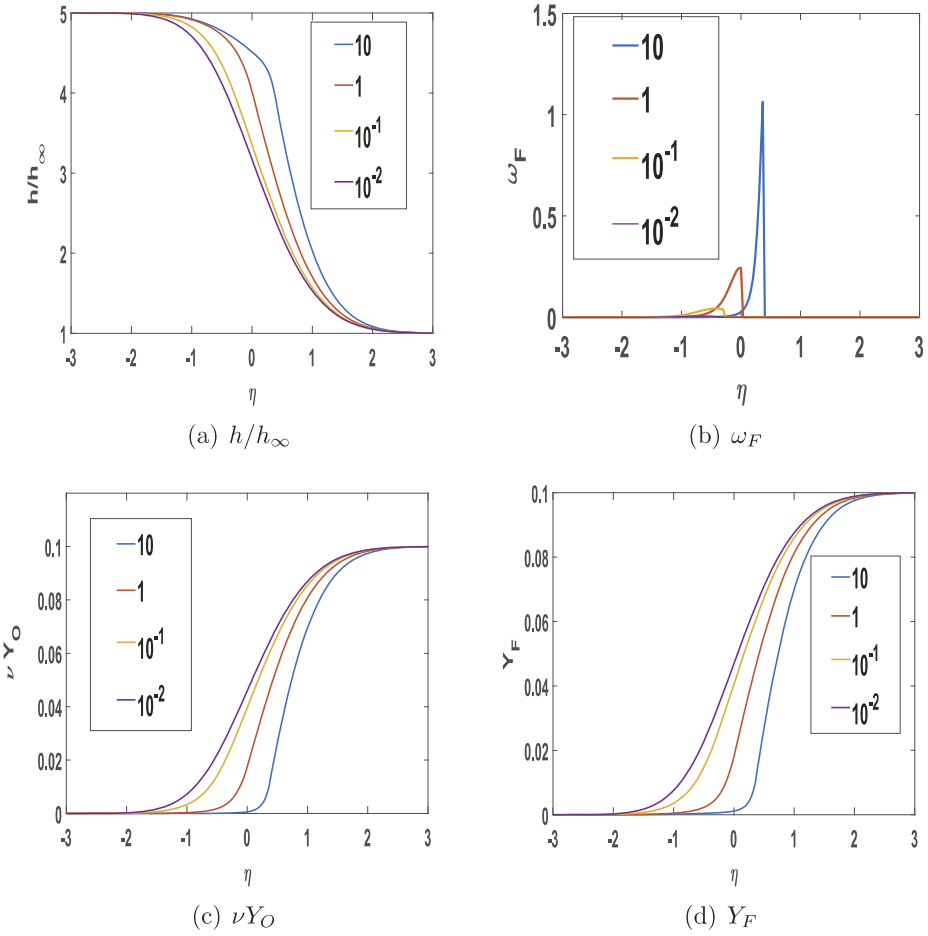

Figure 3. Single premixed flame solutions with several strain-pressure parameter K values for enthalpy h; reaction rate ω_F; and mass fractions $\nu Y_O, Y_F$. $Pr = 1.0; S_1 = 0.25, S_2 = 0.75$.

Diffusion flame and fuel-lean premixed flame

Now, we consider pure propane fuel flowing with negative velocity from the positive-y direction against a lean mixture of propane and oxygen flowing with positive velocity from the negative-y direction. The mixture has $Y_{F,-\infty} = 1/12, Y_{O,-\infty} = 11/12$.

For $K \geq 10^{-1}$, there exist two flames as displayed in Figure 5 and Figure 6: a diffusion flame and, further upstream on the negative-y side, a fuel-lean premixed flame. The diffusion flame has oxygen and fuel approaching from opposite sides while the premixed flame has both reactants coming from the upstream side. Both flames stand at negative values of η or y, on the fuel-lean-mixture side of the interface. The premixed flame stabilizes at a location where the flame speed matches the incoming v velocity magnitude. That flame will be positioned at a larger upstream distance at a higher velocity point as K increases. For example, an increase in pressure would yield a larger burning rate (i.e., larger f flux) and a decrease in strain rate would move the velocity matching point further upstream. As K decreases below that range, the two flames merge into

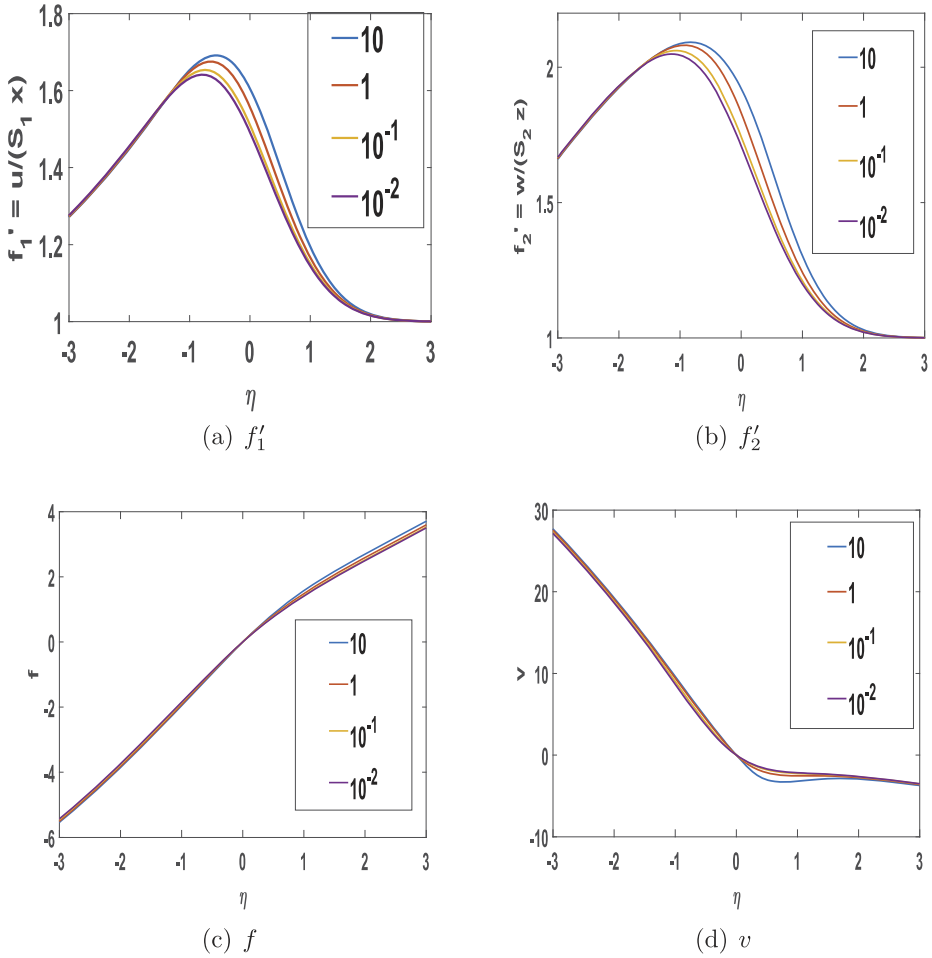

Figure 4. Single premixed flame solutions with several strain-pressure parameter K values for non-dimensional variables f_1', f_2', f, v. $Pr = 1.0; S_1 = 0.25, S_2 = 0.75$.

one diffusion flame. With further decrease in K, extinction occurs. At high K, ω_F is greater for the premixed flame than for the diffusion flame; however, the higher temperature occurs at the diffusion flame. The peak values of ω_F for both flames decrease substantially as merger and extinction occur with decrease of K. Also, the location of the two peaks move closer as merger proceeds with decreasing K.

For high values of K, all of the fuel advecting and diffusing from positive y is consumed at the diffusion flame while all of the fuel advecting and diffusing from negative y is consumed at the premixed flame, leaving a fuel-free region between the two flames. Most of the oxygen flux passes through the premixed flame to reach the diffusion flame via advection and diffusion.

The v component of velocity has a maximum value and a nearly flat profile between the two flames. The consequences of a reaction rate which is nearly second order are seen when we consider an effect of varying the parameter K which is itself monotonically increasing with pressure. As pressure increases, little change in flame speed for the fuel-lean premixed

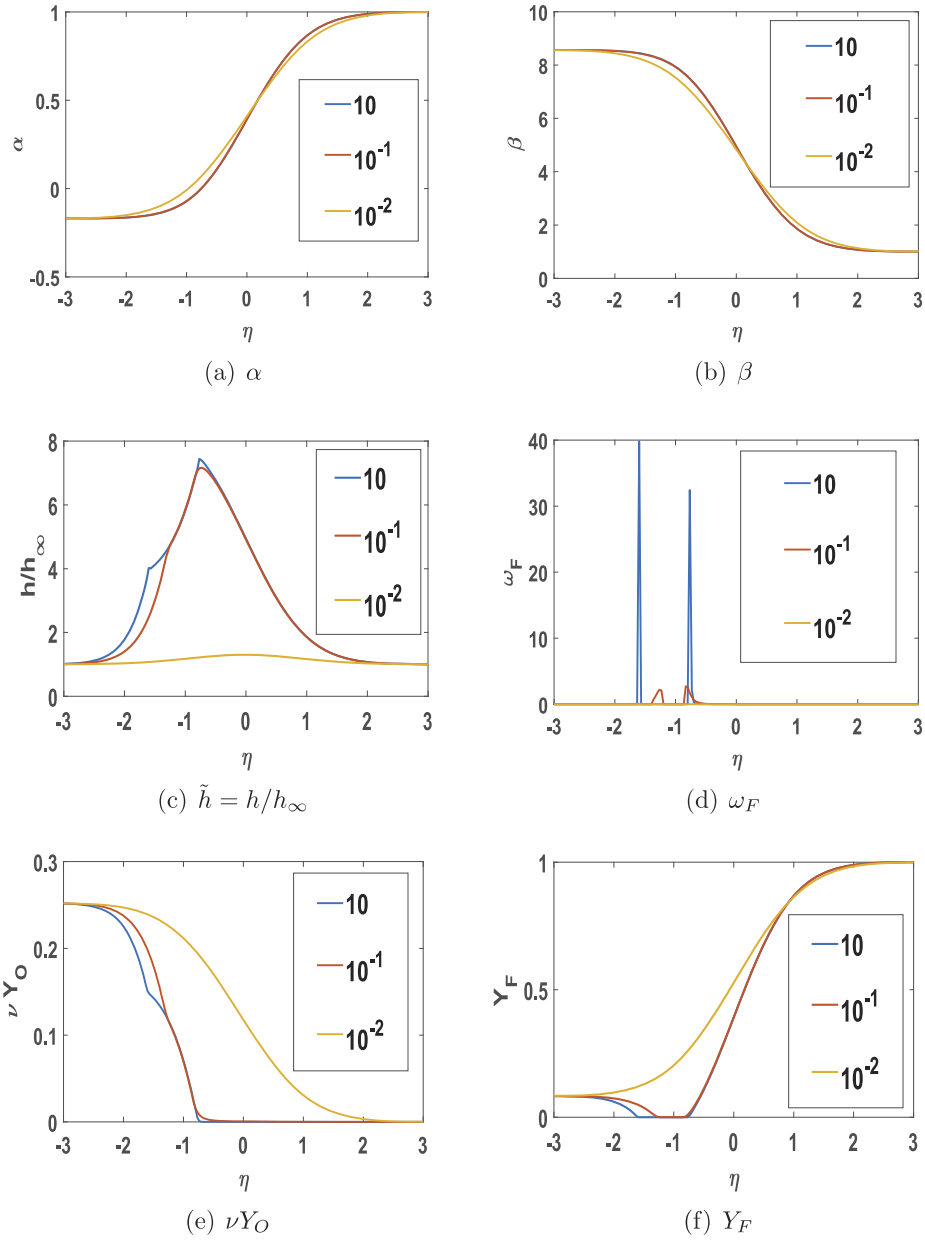

Figure 5. Partially premixed fuel-lean flame plus diffusion flame: two-flame solutions with several strain-pressure parameter K values for nondimensional conserved scalars α, β; enthalpy h; and mass fractions $\nu Y_O, Y_F$. $Pr = 1.0; S_1 = 0.25, S_2 = 0.75$.

flame is seen. However, the mass burning rate reflected through the negative of f does increase with increasing K or pressure. The u and w values peak closer to the interface again.

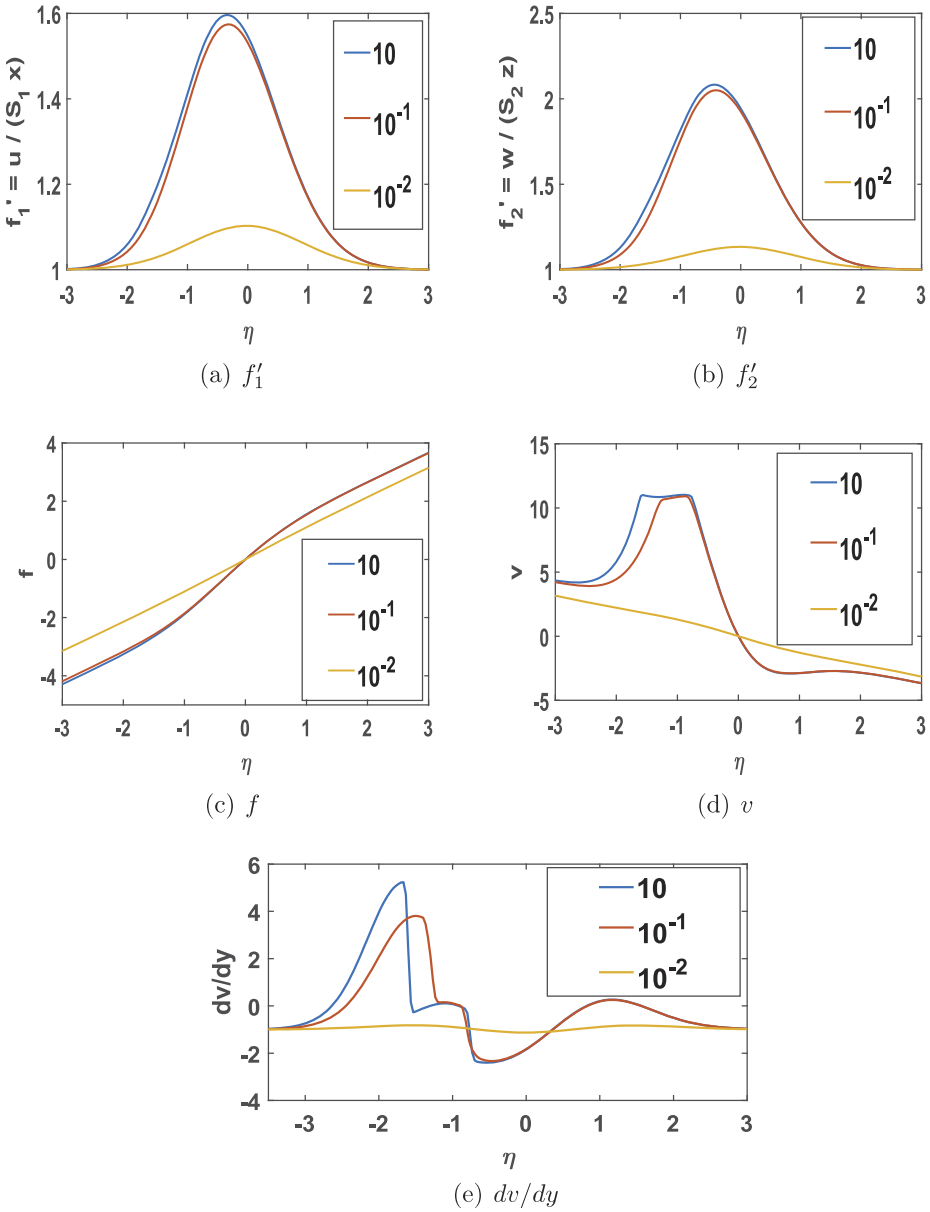

Figure 6. Partially premixed fuel-lean flame plus diffusion flame: two-flame solutions with several strain-pressure parameter K values for nondimensional $f_1', f_2', f, v, dv/dy$. $Pr = 1.0; S_1 = 0.25, S_2 = 0.75$.

Advection is definitely significant in this region between the two flames. The normal strain becomes substantially larger than ambient values close to each of the two flames.

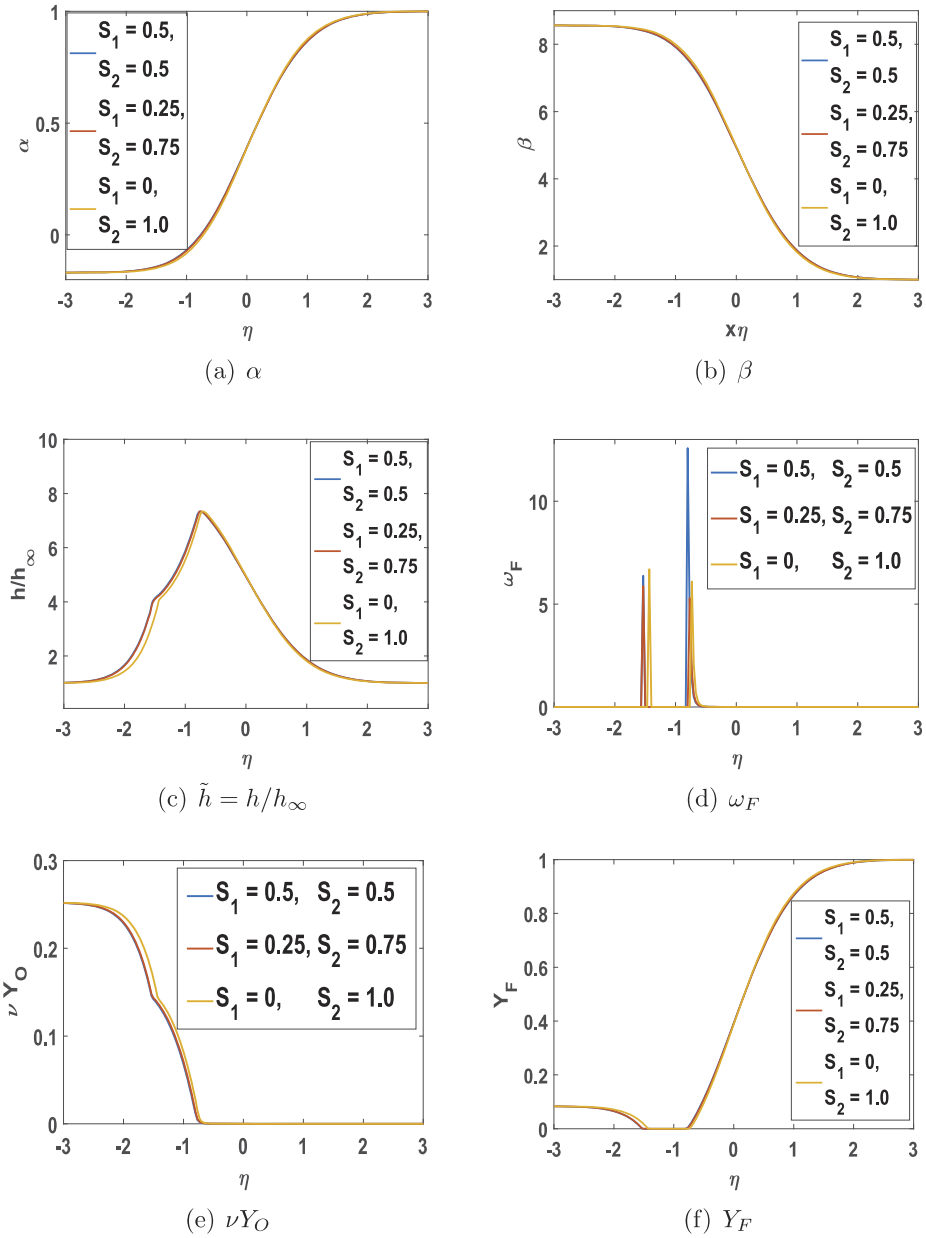

Figure 7. Partially premixed fuel-lean flame plus diffusion flame: two-flame solutions with various strain distributions for nondimensional conserved scalars α, β; enthalpy h; and fractions $\nu Y_O, Y_F$. $Pr = 1.0; K = 1.0$.

Effect of strain-rate distribution

In Figures 7 and 8, we compare three cases with differing distribution of the strain rate in the x and z directions; $S_1 = 0.5, S_2 = 0.5$ (axisymmetric); $S_1 = 0.25, S_2 = 0.75$ (three-dimensional); and $S_1 = 0, S_2 = 1.0$ (planar). The sum of the two ambient transverse strain rates remains fixed

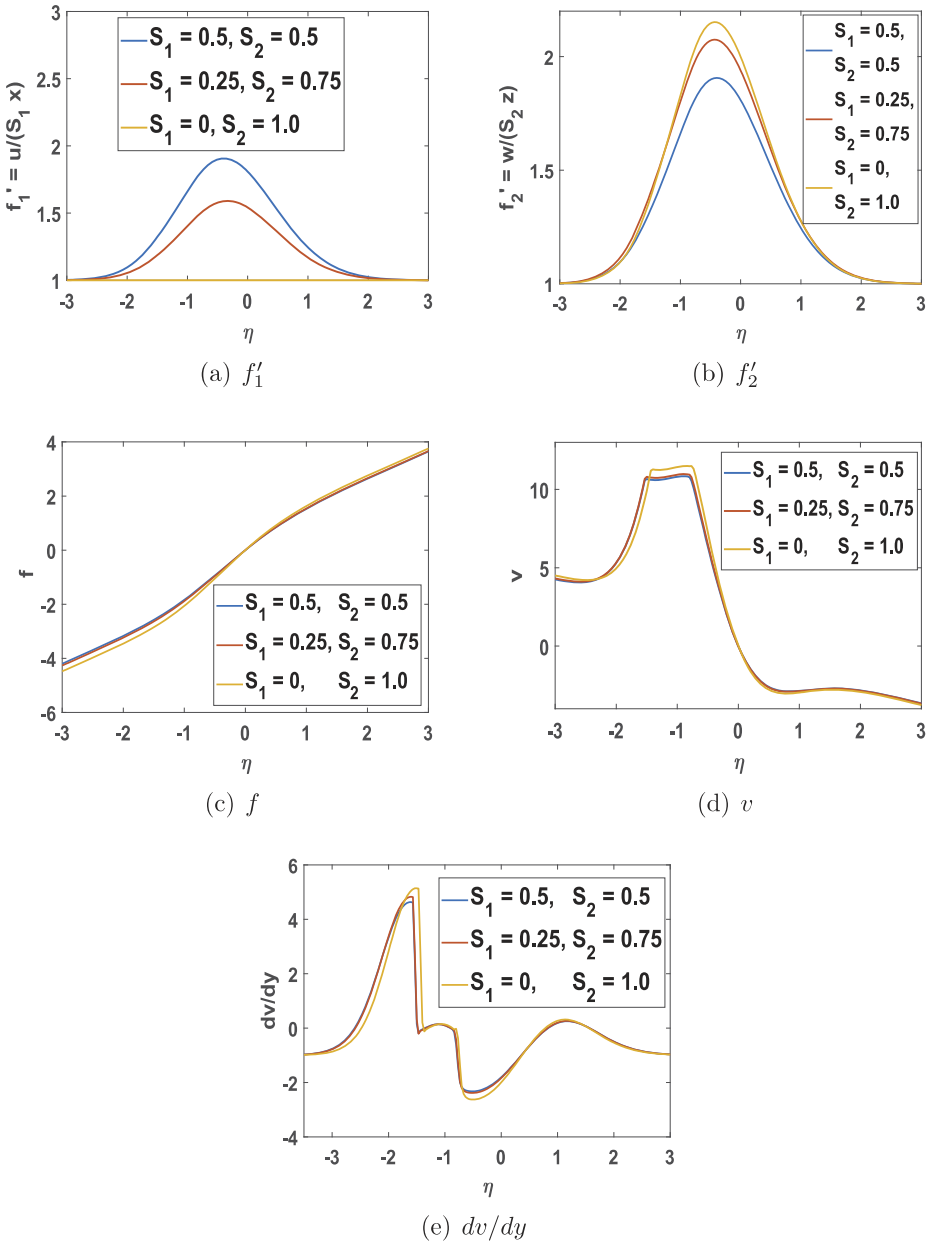

Figure 8. Partially premixed fuel-lean flame plus diffusion flame: two-flame solutions with various strain distributions for nondimensional $f_1', f_2', f, v, dv/dy$. $Pr = 1.0; K = 1.0$.

($K = 1$) and equals the negative of the ambient normal strain in the y direction. The three cases produce very similar results for the scalar variables. The first two cases produce near identical results while the planar case has modestly different results, with a little faster flame speed and mass burning rate. For example, that case brings the two flames closer than for the other cases.

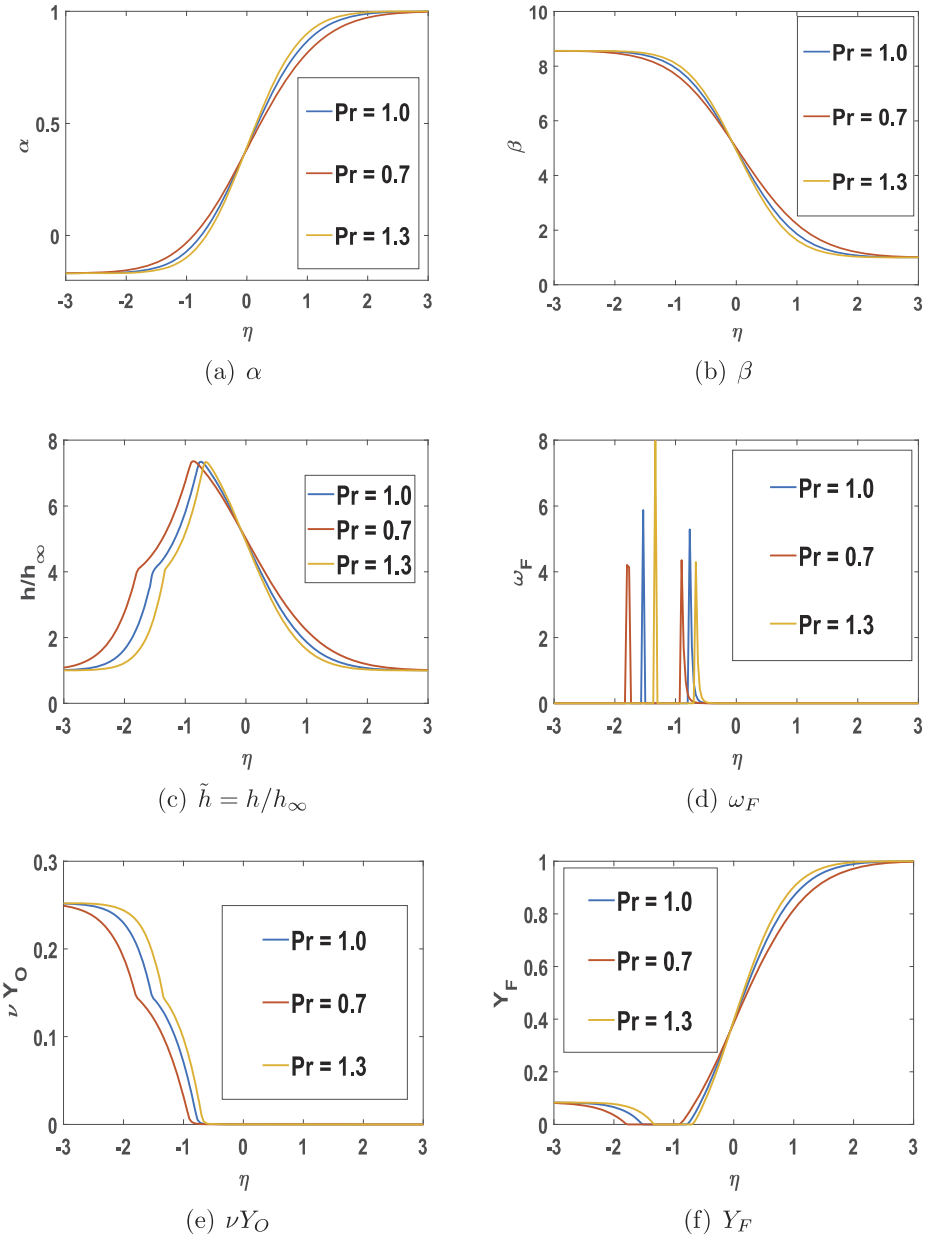

Figure 9. Partially premixed fuel-lean flame plus diffusion flame: two-flame solutions with various Prandtl numbers for nondimensional conserved scalars α, β; enthalpy h; and fractions $\nu Y_O, Y_F$. $K = 1.0; S_1 = 0.25, S_2 = 0.75$.

The v velocity component shows modest influence by the strain-rate distribution as well; the overshoot of the v component is largest in the planar case. u and w experience substantial differences with varying strain-rate distribution, as expected.

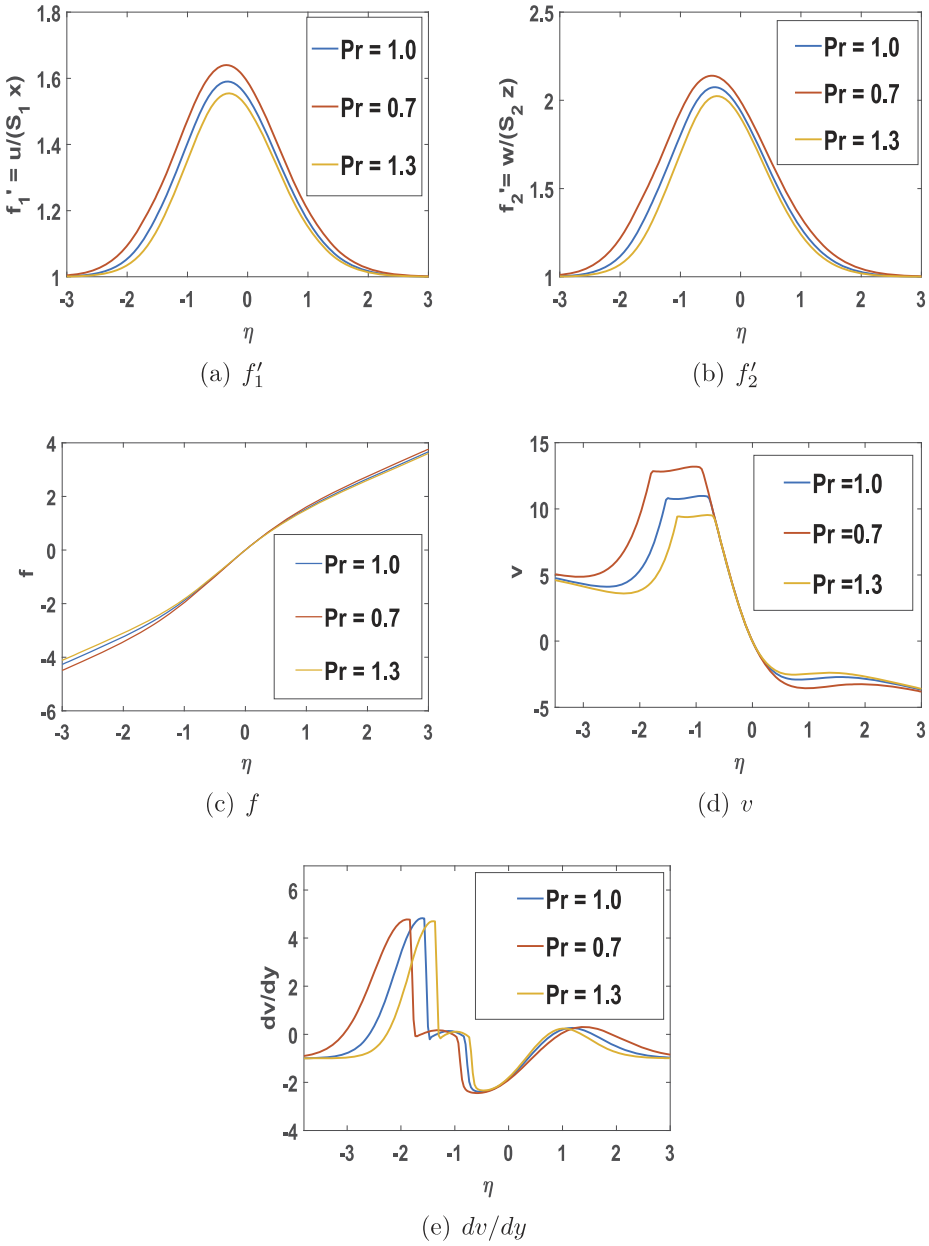

Figure 10. Partially premixed fuel-lean flame plus diffusion flame: two-flame solutions with various Prandtl numbers for nondimensional $f_1', f_2', f, v, dv/dy$. $K = 1.0; S_1 = 0.25, S_2 = 0.75$.

The behaviors identified earlier in this section still occur. For example, flame merging and extinction will occur as the strain rate is increased, i.e., K decreases. The peak magnitudes of the local strain rate dv/dy show some differences, including location which varies with flame location.

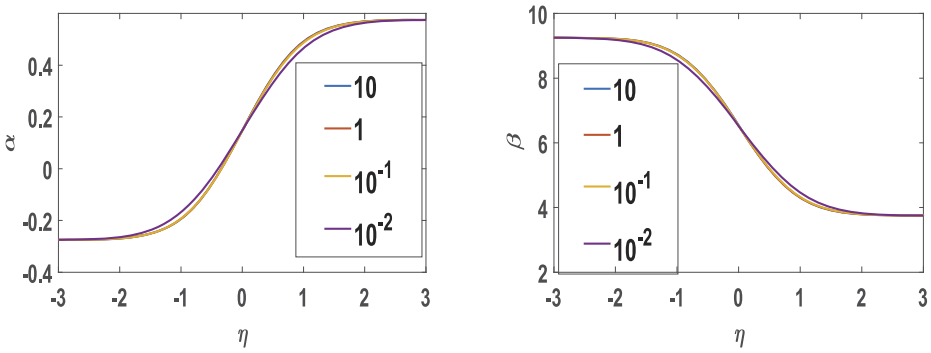

(a) α

(b) β

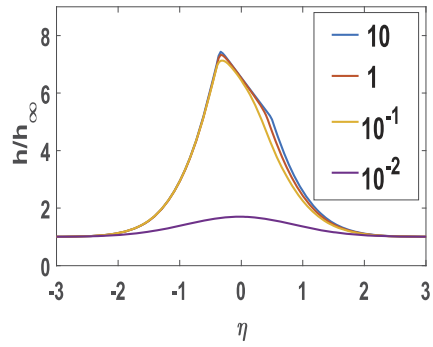

(c) $\tilde{h} = h/h_\infty$

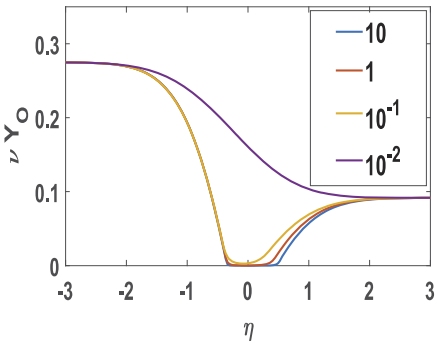

(d) νY_O

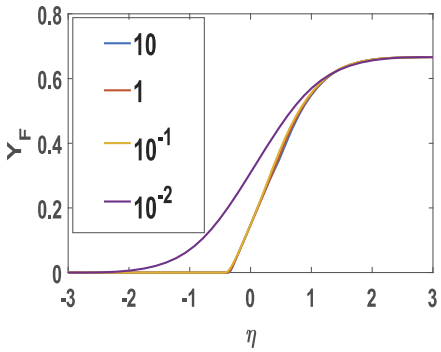

(e) Y_F

Figure 11. Partially premixed fuel-rich flame plus diffusion flame: two-flame solutions with several strain-pressure parameter K values for nondimensional conserved scalars α, β; enthalpy h; and fractions $\nu Y_O, Y_F$. $Pr = 1.0; S_1 = 0.25, S_2 = 0.75$.

Effect of prandtl number

Three cases are studied for Prandtl number with results shown in Figures 9 and 10: $Pr = 0.7, 1.0,$ and 1.3. As Pr increases, the scalar fields experience larger gradients. The premixed

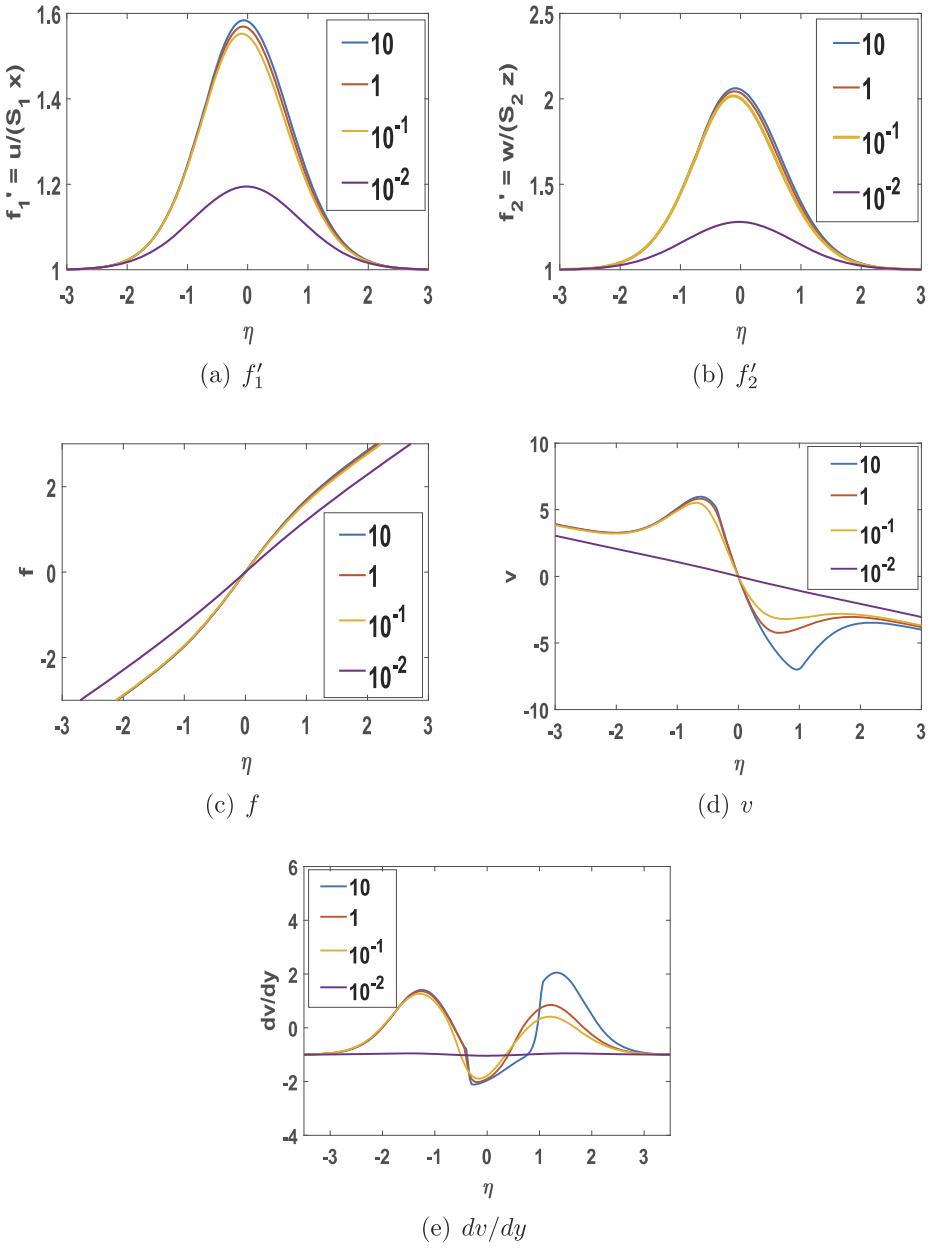

Figure 12. Partially premixed fuel-rich flame plus diffusion flame: two-flame solutions with several strain-pressure parameter K values for nondimensional $f_1', f_2', f, v, dv/dy$. $Pr = 1.0; S_1 = 0.25, S_2 = 0.75$.

flame speed and mass burning rate decrease with increasing Pr. Both the partially premixed flame and the diffusion flame move closer to the counterflow interface with increasing Pr. The fuel-lean premixed flame moves more than the nonpremixed flame so that the two flames come

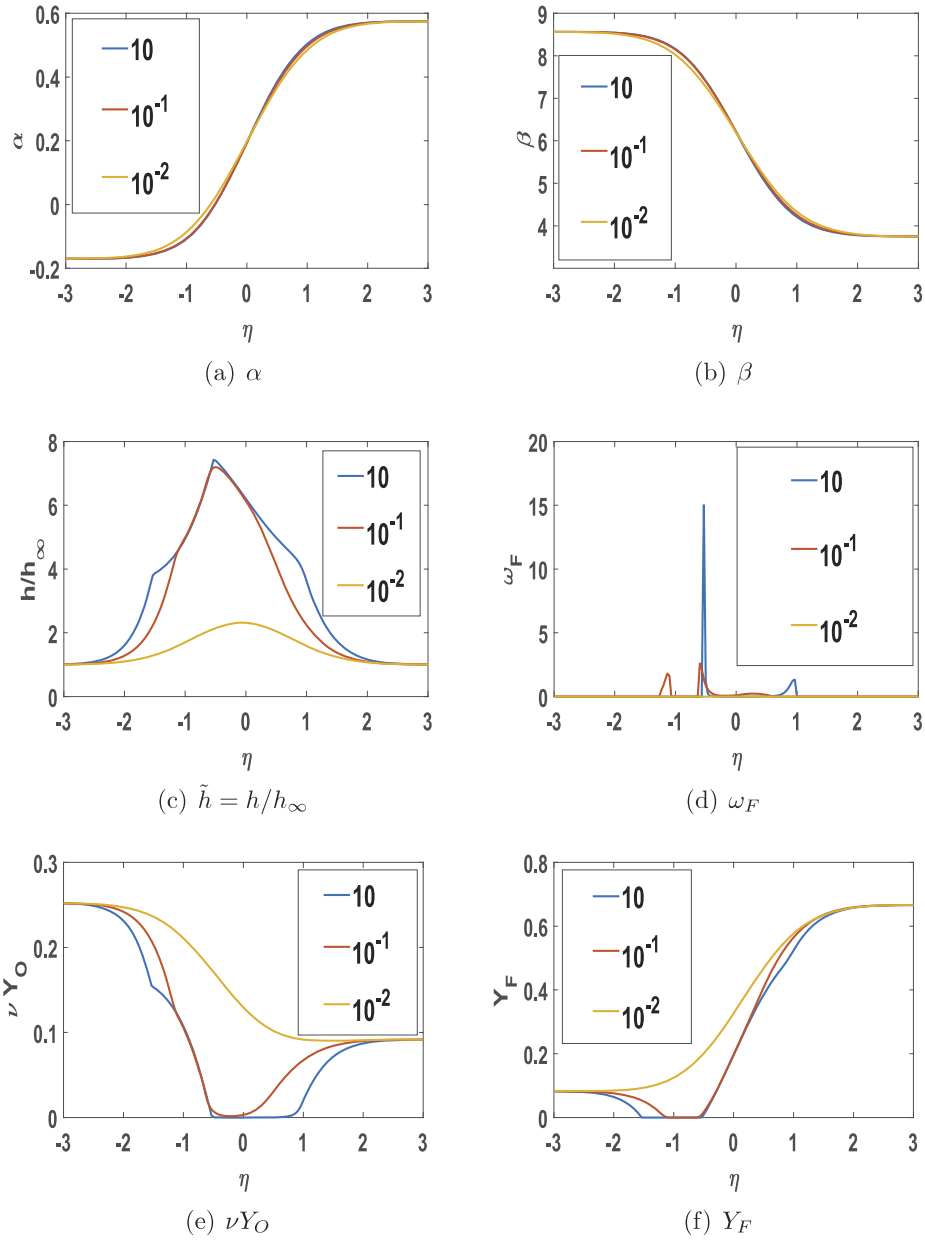

Figure 13. Three-flame solutions with several strain-pressure parameter K values for nondimensional conserved scalars α, β; enthalpy h; and fractions $\nu Y_O, Y_F$. $Pr = 1.0; S_1 = 0.25, S_2 = 0.75$.

closer together but still remain distinct at higher K values. The magnitudes of $f = -\rho v$ also increase as Pr decreases. Velocity overshoot for each component increases as Pr decreases.

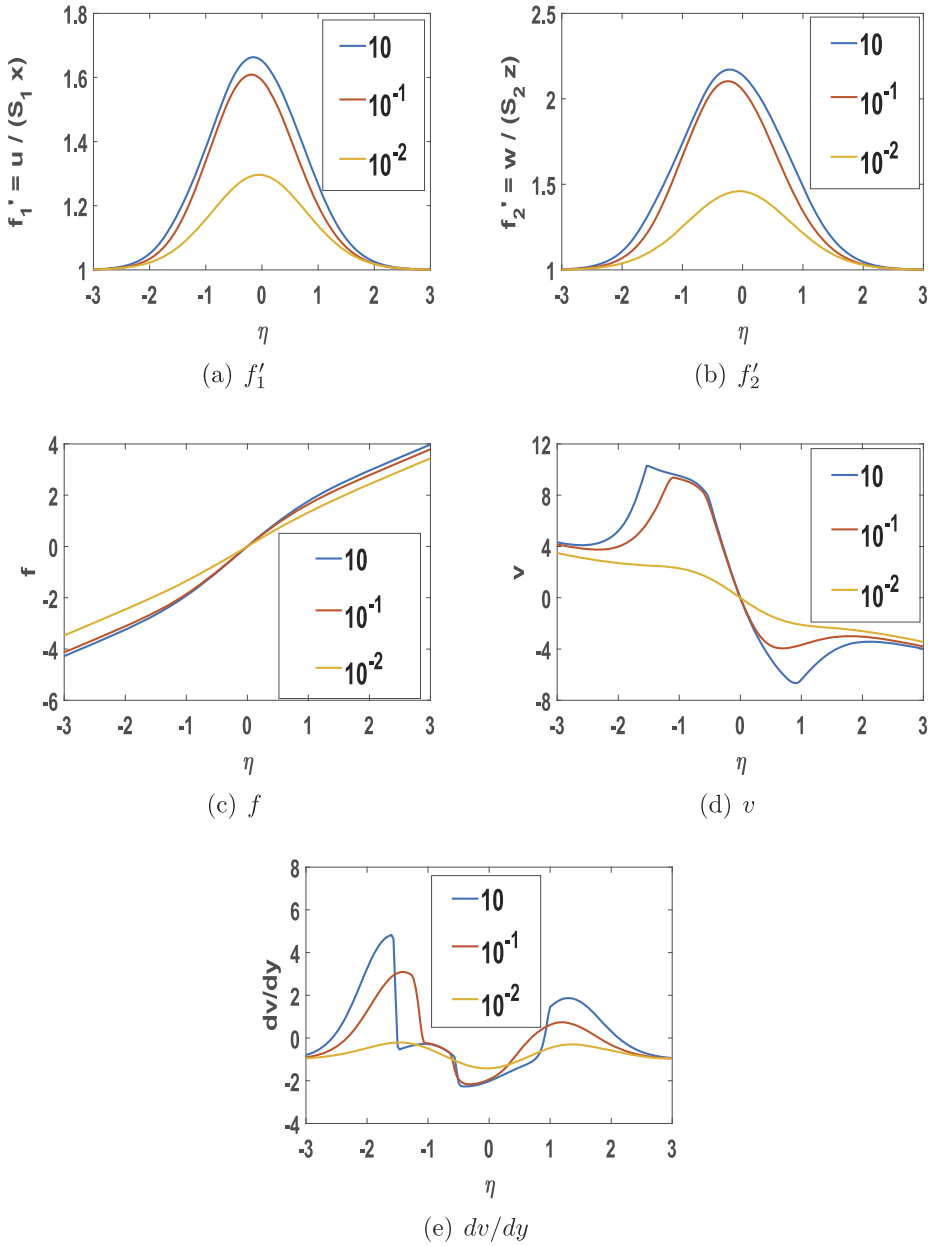

(a) f_1' (b) f_2'

(c) f (d) v

(e) dv/dy

Figure 14. Three-flame solutions with several strain-pressure parameter K values for nondimensional $f_1', f_2', f, v, dv/dy$. $Pr = 1.0; S_1 = 0.25, S_2 = 0.75$.

Diffusion flame and fuel-rich premixed flame

In this section, we examine the case with pure oxygen flowing with positive velocity from the negative-y direction against a rich mixture of propane and oxygen flowing with negative velocity from the positive-y direction. The mixture has

$Y_{F,\infty} = 2/3, Y_{O,\infty} = 1/3$. Here, for the higher K values, two flames are found as shown in Figures 11 and 12: a fuel-rich premixed flame on the positive y side of the interface and a nonpremixed flame on the negative y side. The premixed flame has both fuel and oxygen approaching only from the upstream side while the nonpremixed flame has them approaching from opposite sides. For high values of K, all of the oxygen advecting and diffusing from positive y is consumed at the premixed flame while all of the oxygen advecting and diffusing from negative y is consumed at the diffusion flame, leaving an oxygen-free region between the two flames. Most of the fuel flux passes through the premixed flame to reach the diffusion flame via advection and diffusion.

The premixed flame stabilizes farther upstream with increasing K at a higher velocity and mass flux position, as expected. As K decreases, the distance between the two flames decreases until merger occurs. With greater decrease of K, extinction begins. Velocity overshoot occurs in this case as well.

Three flames

Now, the case is considered with a fuel-rich mixture flowing with negative velocity from the positive-y direction while a fuel-lean mixture flows with positive velocity from the negative-y direction. The fuel-rich mixture has $Y_{F,\infty} = 2/3, Y_{O,\infty} = 1/3$ and the fuel-lean mixture has $Y_{F,-\infty} = 1/12, Y_{O,-\infty} = 11/12$. Results are shown in Figures 13 and 14.

Again, the tendency remains for merging and extinction to occur as K is reduced. First, the fuel-rich premixed flame merges with the diffusion flame. Then, with further decrease, the fuel-lean flame merges with the diffusion flame. At still lower K, extinction occurs. The two premixed flames are each stationed farther upstream at a higher velocity point as K increases. These results are consistent with the experiments of Hamins, Thridandam, and Seshadri (1985) but contradict Rajamanickam et al. (2019) who find in the triple-flame structure that the fuel-lean flame merges first with the diffusion flame. However, they use uni-molecular one-step kinetics which Westbrook and Dryer (1984) show overestimate flame speed away from the stoichiometric condition, especially on the fuel-rich side.

For high values of K, all of the oxygen advecting and diffusing from positive y is consumed at the fuel-rich premixed flame while the oxygen advecting and diffusing from negative y is partially consumed at the fuel-lean premixed flame with the rest consumed at the diffusion flame, leaving an oxygen-free region between the fuel-rich premixed flame and the diffusion flame. Most of the oxygen flux passes through the fuel-lean premixed flame to reach the diffusion flame via advection and diffusion. In a similar fashion, all of the fuel advecting and diffusing from negative y is consumed at the fuel-lean premixed flame while the fuel advecting and diffusing from positive y is partially consumed at the fuel-rich premixed flame with the rest consumed at the diffusion flame, leaving a fuel-free region between the fuel-lean premixed flame and the diffusion flame. Most of the fuel flux passes through the fuel-rich premixed flame to reach the diffusion flame via advection and diffusion.

Presentation in Σ space

Flamelet theory (Peters 2000; Pierce and Moin 2004) has evolved with the use of a conserved scalar as the independent variable replacing the y or η coordinate. Bilger (1976) has emphasized the use of element-based mass fractions which become conserved scalars because chemistry does not destroy atoms but only changes molecules. Bilger refers to it as a "mixture fraction". This allows us to consider general chemical kinetics without the use of the one-step assumption. Define the element mass fraction for the atom identified by integer k as $Y_k \equiv \Sigma_{m=1}^{N} a_{m,k} Y_m W_k / W_m$, where $a_{m,k}, W_k,$ and W_m are the integer number of k atoms in molecule m, the atomic weight of k, and the molecular weight of m, respectively. Then, Y_k is a conserved scalar satisfying the homogeneous form (i.e., without reaction rate) of the differential equation given by Equation (5) for either the steady state or unsteady state. It only is useful as a replacement for y if it remains monotonic in y. That will be always true for the steady state; however, in the unsteady case, monotonic behavior of the initial conditions becomes a requirement.

Thus, the use of a variable only related to fractions of chemical species or of atomic species is not the best fundamental starting point. Firstly, there is no need for the conserved scalar to have any physical meaning. Secondly, the use of molecular species to construct the conserved scalar can fail with multiple flames in both the steady and unsteady states to meet the monotonic condition of a normalized variable to replace y or η as the independent variable. Thirdly, the use of atomic species to construct the conserved scalars can fail with single or multiple flames in the unsteady state to meet the monotonic condition. So, a more general approach is offered.

First, the steady state is considered. A simple option is to use the solution Σ of the following equation and boundary conditions:

$$\begin{aligned} \Sigma'' + Pr(S_1 f_1 + S_2 f_2)\Sigma' = 0 \\ \Sigma(\infty) = 1 \; ; \quad \Sigma(-\infty) = 0 \end{aligned} \tag{17}$$

The result is

$$\begin{aligned} \Sigma(\eta) &= \frac{J(\eta)}{J(\infty)} \\ J(\eta) &\equiv \int_{-\infty}^{\eta} e^{-I(\eta')} d\eta' \\ I(\eta) &\equiv \int_{-\infty}^{\eta} Pr[S_1 f_1(\zeta) + S_2 f_2(\zeta)] d\zeta \end{aligned} \tag{18}$$

It is advisable to use the steady form of Σ defined above, even for the unsteady problem. In that unsteady case, f_1 and f_2 should be taken from the steady solution since the density within the η definition would otherwise vary with time, the true solutions for unsteady f_1 and f_2 would not satisfy the steady equations utilized here, and possibly S_1^* and S_2^* might vary with time.

In similar fashion to Peters (2000), the independent variables t and y can be replaced by $\tau \equiv t$ and $\Sigma(y)$ in Equation (5). The steady-state result is

$$
\begin{aligned}
&2\chi\frac{d^2Y_m}{d\sum^2}+\Pr\omega_m=0;m=1,2,\ldots\ldots,N\\
&\chi\frac{d^2\tilde{h}}{d\Sigma^2}+Pr\tilde{Q}\omega_m=0\\
&\chi\equiv\frac{1}{2}\left(\frac{d\Sigma}{d\eta}\right)^2=\frac{1}{2\rho^2}\left(\frac{d\Sigma}{dy}\right)^2=\frac{1}{2}\frac{e^{-2I(\eta)}}{J^2(\infty)}
\end{aligned}
\tag{19}
$$

where χ is commonly named the scalar dissipation rate. However, for laminar flows, it is better described as a measure of the strain rate. In Equation (19), $\eta(\Sigma)=J^{Inv}(\Sigma J(\infty))$ must be substituted where J^{Inv} is the inverse function of J which must be determined numerically or approximated. In a special case (Peters 2000) where f_1 and f_2 are linear in η obtained through a constant-density assumption, J becomes an error function because the velocity component v becomes linear in η (and in y). However, when density varies across the counterflow, a linear behavior cannot occur.

Obviously, Σ equals a normalized steady-state conserved scalar. For example,

$$
\Sigma=\frac{\alpha(\eta)-\alpha(-\infty)}{\alpha(\infty)-\alpha(-\infty)}=\frac{\beta(\eta)-\beta(-\infty)}{\beta(\infty)-\beta(-\infty)} \tag{20}
$$

These results apply for the simple counterflow diffusion flame as well as for a more complex counterflow with multiple flame. For the diffusion flame case with oxygen and fuel only coming in opposing flows, the mixture fraction Z commonly used is simply the normalized α conserved scalar. Thereby, $Z=\Sigma$ in that case; however, in a broader set of problems, they are not always the same.

In the steady state, the reaction rate in Equation (19) is determined from the mass fractions using the known linear relations among temperature (from enthalpy for constant c_p), mass fractions, and the conserved scalars $\Sigma, \alpha,$ and β. So, a solution can be found in Σ-space. For the steady state with fast chemical kinetics, $\omega_m(\Sigma)$ will have significant value within a narrow region in Σ-space around the stoichiometric value. On both sides of that narrow region, Y_m will be linear in Σ.

The solution for a simple counterflow diffusion flame is given in Figure 15. Σ is shown as a monotonic function of η. The functions $\tilde{h}, vY_O,$ and Y_F of Σ have linear segments except for curved portions where the chemical reaction is occurring. Similar principles hold for the behavior in Σ space with three flames as shown in Figure 16. Of course, now, there are three reaction zones and four line segments connecting them in high K cases. In the multiple-flame case, merging of flames is seen as K decreases, reducing the number of line segments. For all configurations, the reaction zones broaden as K decreases, increasing the curvature of the lines in the plots.

For the steady-state case, the results are equivalent to Bilger's approach using atomic species. Note that the formulation with Σ or Z is not convenient in the premixed-flame case since those parameters are uniform functions of η in the steady-state case.

Let us now consider the unsteady case. The mass fraction $Y_m(y,t)$ and the scalar $\Sigma(y)$ are governed by the differential equations:

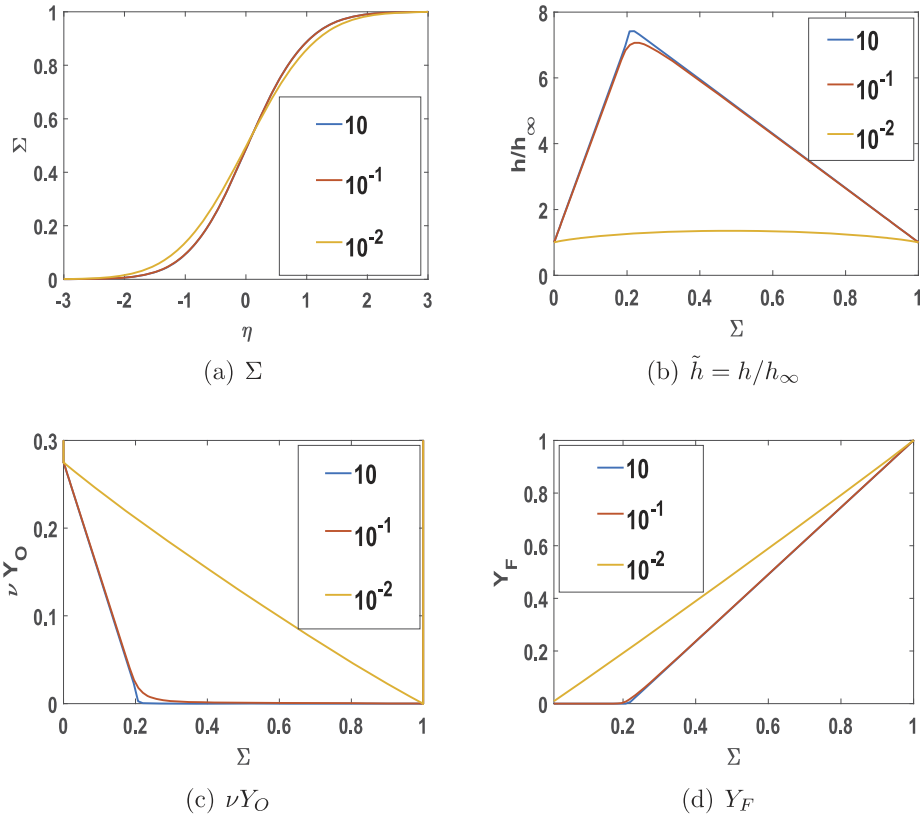

Figure 15. Single diffusion flame solutions with several strain-pressure parameter K values for non-dimensional Σ vs. η; $h, \nu Y_O, Y_F$ vs. Σ. $Pr = 1.0; S_1 = 0.25, S_2 = 0.75$.

$$\frac{\partial Y_m}{\partial t} + \mathrm{v}\frac{\partial \mathrm{Y_m}}{\partial \mathrm{y}} = \frac{\partial}{\partial \mathrm{y}}\left(\mathrm{D}\frac{\partial \mathrm{Y_m}}{\partial \mathrm{y}}\right) + \omega_\mathrm{m}; \mathrm{m} = 1, 2, \ldots, \mathrm{N}$$
$$\mathrm{v_s}\frac{d\Sigma}{dy} = \frac{d}{dy}\left(D\frac{dY_m}{dy}\right)\ ;\ \Sigma(\infty) = 1\ ;\ \Sigma(-\infty) = 0 \tag{21}$$

where $\mathrm{v_s}$ is a function of y only. The transformation of coordinates using $\Sigma(y)$ yields

$$\frac{\partial Y_m}{\partial t} + (\mathrm{v} - \mathrm{v_s})\frac{\partial \mathrm{Y_m}}{\partial \Sigma} = \left(\frac{\mathrm{d}\Sigma}{\mathrm{dy}}\right)^2 \frac{\partial}{\partial \Sigma}\left(\mathrm{D}\frac{\partial \mathrm{Y_m}}{\partial \Sigma}\right) + \omega_\mathrm{m}\ ;\ \mathrm{m} = 1, 2, \ldots., \mathrm{N} \tag{22}$$

For cases where the flow field has steady velocity, $\mathrm{v_s} = \mathrm{v}$ can be taken and the term for the first derivative in Σ space disappears. The behavior of Σ is then still described by Equation (18). This would imply an unsteady behavior for the mass fractions at a faster timescale than exists for velocity and density. For the case where velocity and density vary as swiftly as mass fraction, a nonphysical $\mathrm{v_s}(y)$ function must be used, complicating somewhat the PDE for Y_m in Σ space. In fact, the advantage of Σ space is lost, once the advective (i.e., first-derivative) term remains in the PDE. If v were time

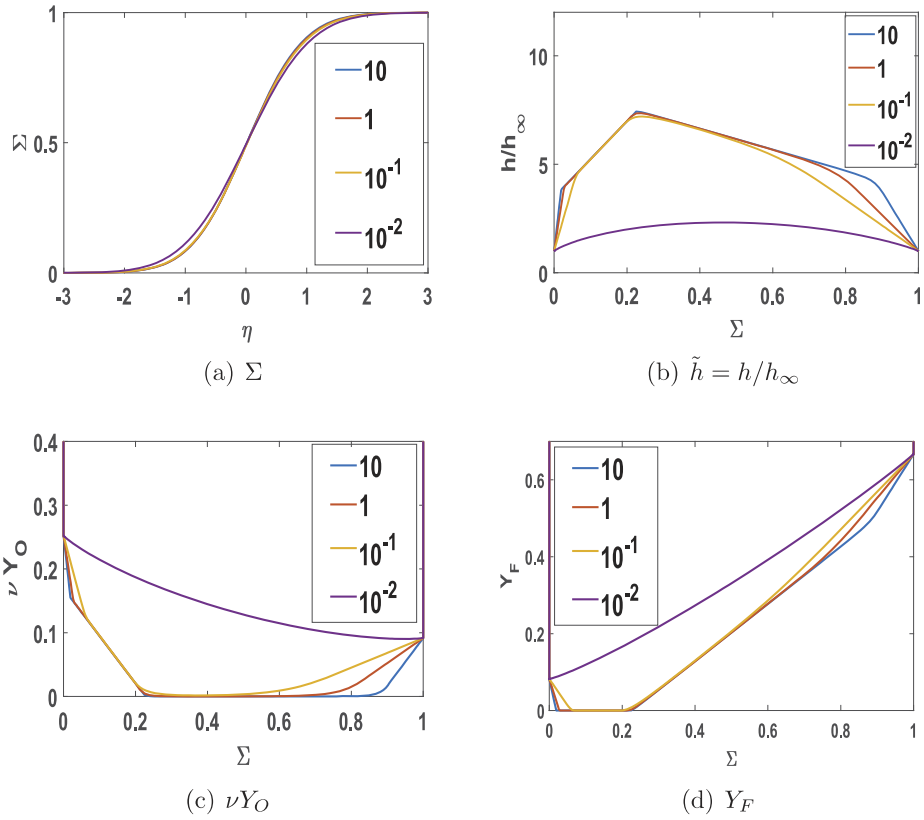

(a) Σ (b) $\tilde{h} = h/h_\infty$

(c) νY_O (d) Y_F

Figure 16. Three-flame solutions with several strain-pressure parameter K values for nondimensional Σ vs. η; $h, \nu Y_O, Y_F$ vs. Σ. $Pr = 1.0; S_1 = 0.25, S_2 = 0.75$.

dependent and $v_s \equiv v$, the advective term in Equation (22) disappears leaving a simpler relation for the scalar Y_m. However, Σ becomes time dependent and the ordinary differential relation for Σ in Equation (21) is replaced by a partial differential equation with a time-derivative term.

Concluding remarks

Viscous, reacting counterflows are analyzed with three-dimensional normal strain rate. A similar system of the Navier-Stokes equations coupled with equations for scalar transport is developed and solved. Variable density, temperature, and composition are considered. Results for planar flows and axisymmetric flows are obtained as limits here. The boundary-layer approximation is not required.

In steady, variable-density configurations, a set of ODEs govern the two transverse velocity profiles. Each of the three velocity components as well as the diffusion rates for mass and energy depend on the two normal strain rates parallel to the counterflow interface or the wall and thereby not merely on the sum of those two strain rates.

The Damköhler number *Da* is an important parameter for both the determination of the number of flames in the stable configuration and the extinction process. It is a ratio of residence time to chemical time where the residence time is the reciprocal of the strain rate. As *Da* increases, a larger number of independent flames become possible in the case where a fuel-lean combustible mixture and a fuel-rich combustible mixture are in counterflow. For high *Da* values, a fuel-lean premixed flame, diffusion flame, and fuel-rich premixed flame can occur for the propane-oxygen mixtures. With decreasing *Da*, the fuel-rich flame and the diffusion flame merge into a diffusion flame. With greater decrease, the fuel-lean flame merges and one diffusion flame remains. After still greater decrease, extinction occurs. *Da* has been varied over four orders of magnitude here. With pure oxygen and a fuel-rich combustible mixture in counterflow, the high *Da* behavior has a diffusion flame and a fuel-rich premixed flame which merge into a diffusion flame at lower *Da*. With pure fuel and a fuel-lean combustible mixture in counterflow, the high *Da* behavior has a diffusion flame and a fuel-lean premixed flame which merge into a diffusion flame at lower *Da*. For these two-flame situations, continued reduction of *Da* results in extinction of the diffusion flame.

The multiple-flame structures here are believed to be related to flows with triple flames. The merging of branches of triple flames has been observed by Nguyen, Popov, and Sirignano (2018) and Nguyen and Sirignano (2018). It has also been seen in some unpublished work on triple flames with methane-oxygen mixtures undergoing three-dimensional strained flow.

The impact of the magnitude of the dimensional strain rate is made solely through *Da*. The effect of strain-rate distribution is generally greater on the transverse velocity components, *u* and *w*, than on the incoming velocity component, v, or the scalar variables. The velocity profiles and the scalar profiles are shown to depend on the Prandtl number as well as the strain rates.

Important corrections are shown for existing approaches which are based on a constant-density assumption. Velocity overshoots are seen in the viscous layer for all three velocity components.

For the case of a single premixed flame in counterflow, the reactive-diffusive segment of the flame structure moves into the opposing stream as strain rate increases and/or pressure decreases, while the diffusive-advective segment remains in the stream bringing the combustible mixture.

The calculations were performed by setting $\omega_F = 0$ below a prescribed temperature so that reactions would not occur far upstream (thereby addressing the cold-boundary problem). The choice of threshold value for temperature made no qualitative difference in the results. There were insignificant quantitative differences in the diffusion-flame location or its peak temperature. However, there were some differences in the location and flame temperature for the premixed flames.

Flamelet theory as a closure model for turbulent combustion is based on the tracking of two variables: a normalized conserved scalar Z and the strain rate, either directly or through a progress variable. Two significant new findings are relevant. Firstly, the concept of the mixture fraction as the normalized conserved scalar has to be generalized to account for situations with multiple branches for the flamelet.

A new normalized scalar is needed which generalizes the mixture fraction used for the single diffusion flame; The variable Σ is presented for the more general case; it is built on the Shvab-Zel'dovich conserved scalars. Secondly, additional parameters must be tracked to account for variable equivalence ratios of the combustible mixtures. That is, the ambient compositions cannot be assumed to be pure fuel or pure oxidizer.

Nomenclature

c_p	Specific heat under constant pressure $J/(^oKkg)$
c_v	Specific heat under constant volume $J/(^oKkg)$
D	Mass diffusivity m^2/s
Da	Damköhler number
h	Specific enthalpy J/kg
$h_{f,m}$	Heat of formation for species m J/kg
K	Ratio for Damköhler number
$Le = \lambda/(c_p\rho D)$	Lewis number
N	Number of species
p	Pressure N/m^2
Pr	Prandtl number
Q	Fuel heating value J/kg
R	Specific gas constant $J/(^oKkg)$
R_u	Universal gas constant $J/(^oKmole)$
S_1	Normal strain rate in x direction s^{-1}
S_2	Normal strain rate in z direction s^{-1}
t	Time s
u, v, w	Velocity components m/s
x, y, z	Cartesian coordinate (m)
Y_m	Mass fraction of species m
α, β	Shvab-Zel'dovich conserved scalars
η	Density-weighted coordinate kg/m^2
ν	Mass stoichiometric ratio
λ	Thermal conductivity $J/(sm^2)$
ρ	Density kg/m^3
ω_m	Reaction rate for species s^{-1}
Σ	Normalized conserved scalar
τ_{ij}	Viscous stress tensor N/m^2
Superscripts	
*	Dimensional values
$'$	Ordinary derivative
Subscripts	
i, j, k	Integers for vector and tensor component designation
m	Integer for species designation
∞	Conditions at positive infinite y
$-\infty$	Conditions at negative infinite y

Disclosure statement

No potential conflict of interest was reported by the author.

Funding

This research was supported by the Air Force Office of Scientific Research under Grant FA9550-18-1-0392 with Dr Mitat Birkan as the scientific officer.

References

Bilger, R. W. 1976. The structure of diffusion flames. *Combust. Sci. Technol.* 13:155–70. doi:10.1080/00102207608946733.

Cetegen, B. M., and W. A. Sirignano. 1988. Study of molecular mixing and a finite rate chemical reaction in a mixing layer. *Proceedings of Twenty-Second Symp. (Int.) Combust.* 489–94. Pittsburgh, PA: Combustion Institute.

Cetegen, B. M., and W. A. Sirignano. 1990. Study of mixing and reaction in the field of a vortex. *Combust. Sci. Technol.* 72:157–81. doi:10.1080/00102209008951646.

Hamins, A., H. Thridandam, and K. Seshadri. 1985. Structure and extinction of a counterflow partially premixed, diffusion flame. *Chem. Eng. Sci.* 40:2027–38. doi:10.1016/0009-2509(85)87020-2.

Karagozian, A. R., and F. E. Marble. 1986. Study of a diffusion flame in a stretched vortex. *Combust. Sci. Technol.* 45:65–84. doi:10.1080/00102208608923842.

Linan, A. 1974. The asymptotic structure of counterflow diffusion flames for large activation energies. *Acta Astonautica* 1:1007–39. doi:10.1016/0094-5765(74)90066-6.

Marble, F. E. 1985. Growth of a diffusion flame in the field of a vortex. In *Recent Advances in the Aerospace Sciences*, 395–413. New York: Plenum Press.

Nguyen, T., P. Popov, and W. A. Sirignano. 2018. Longitudinal combustion instability in a rocket motor with a single coaxial injector. *J. Propul. Power* 34 (2):354–73. doi:10.2514/1.B36516.

Nguyen, T., and W. A. Sirignano. 2018. The impacts of three flamelet burning regimes in nonlinear combustion dynamics, invited paper. *Combust. Flame* 195:170–82. doi:10.1016/j.combustflame.2018.03.031.

Peters, N. 2000. *Turbulent Combustion*. 1st ed. Cambridge, UK: Cambridge University Press.

Pierce, C., and P. Moin. 2004. Progress-variable approach for large-eddy simulation of non-premixed turbulent combustion. *J. Fluid Mech.* 504:73–97. doi:10.1017/S0022112004008213.

Rajamanickam, P., W. Coenen, A. L. Sanchez, and F. A. Williams. 2019. Influences of stoichiometry on steadily propagating triple flames in counterflows. *Proc. Combust. Inst.* 37:1971–77. doi:10.1016/j.proci.2018.05.044.

Sirignano, W. A. 2019. Counterflow and wall stagnation flow with three-dimensional strain. *Phys. Fluids* 31:053605. doi:10.1063/1.5096472.

Westbrook, C. K., and F. L. Dryer. 1984. Chemical kinetic modeling of hydrocarbon combustion. *Prog. Energy Combust. Sci.* 10 (1):1–57. doi:10.1016/0360-1285(84)90118-7.